CLAS12 FTOF Panel-1a and Panel-2 Refurbishment and Baseline Test Results

D.S. Carman, Jefferson Laboratory

ftof-1a-2-qa.tex

June 4, 2013

Abstract

This write-up details the refurbishment work completed in 2012 and 2013 on the CLAS12 FTOF panel-1a and panel-2 arrays. In addition the procedures and results from the high voltage calibrations and the time-resolution measurements are explained and detailed.

1 FTOF Overview

The Forward Time-of-Flight System (FTOF) will be a major component of the CLAS12 forward detector used to measure the time-of-flight of charged particles emerging from interactions in the target. The average path length from the target to the FTOF counters will be roughly 7 m. The requirements for the FTOF system include excellent timing resolution for particle identification and good segmentation for flexible triggering options and to minimize the average counting rate per detector element. The system specifications call for a time resolution of σ_{TOF}=80 ps at the more forward angles of CLAS12 and 150 ps at angles larger than 35°. The system must also be cable of operating in a high-rate environment. The maximum counting rate occurs in the forward direction where, at an operating luminosity of 1×10^{35} cm^{-2}s^{-1}, the average rate per scintillator is approximately 250 kHz.

In order to meet the requirements for the tight timing resolution, the major considerations in the design of the FTOF system are:

Scintillator Size: The width of each scintillator determines the granularity of the scattering angle definition in the trigger. Also, the overall size of the system demands careful consideration of light collection in order to optimize the time resolution of the system.

Geometry: The projected space behind the coils of the main CLAS12 torus is inactive and therefore useful for locating the light guides, photomultiplier tubes (PMTs), voltage dividers, and cables. The remaining area in the forward direction is the fiducial region of the detector and must be covered with scintillator counters.

Magnetic Field: The PMTs must be properly shielded from the stray magnetic fields of the CLAS12 torus. The maximum fields are expected to be at the level of ∼30 G.

In each of the six sectors of CLAS12, the FTOF system will be comprised of three sets of TOF counters, referred to as panels. They have been named panel-1a, panel-1b, and panel-2. Each panel consists of an array of rectangular scintillators with a PMT on each end. Panel-1 refers to the sets of counters located at forward angles (roughly 5° to 35°) (where two panels are necessary to meet the 80 ps average time resolution requirement) and panel-2 refers to the sets of counters at larger angles (roughly 35° to 45°). The positioning and attachment of the FTOF system panels to the Forward Carriage of CLAS12 are shown in Fig. 1. Each of the six panel-1a arrays contains 23 counters. The new highly segmented panel-1b arrays contain 62 counters. Finally, each panel-2 array consists of 5 counters.

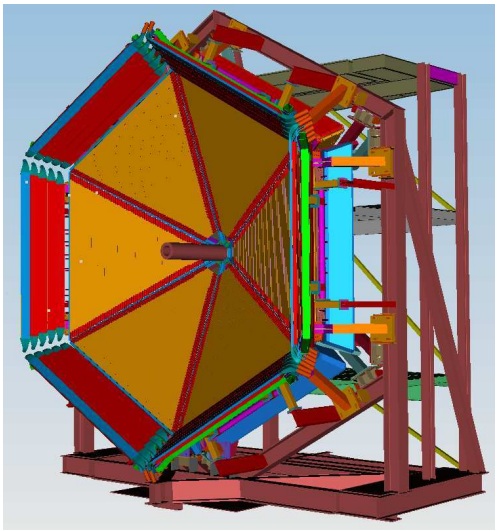

Figure 1: View of the FTOF counters for CLAS12 highlighting the location of the panel-1 and panel-2 counters. The panel-1b counter arrays are shown in orange and the panel-2 counter arrays shown in red are mounted around the perimeter of the Forward Carriage. The panel-1a counter arrays mounted just downstream of the panel-1b arrays are not visible in this picture. The Forward Carriage is roughly 10 m across.

The FTOF counter arrays in the angular range from 5° to 35° will consists of two sets of six triangular arrays. Just upstream of the new Preshower Calorimeter (PCAL) detectors the so-called panel-1a arrays will be mounted. These detector sets were refurbished from the panel-1 TOF counters from the recently decommissioned CLAS spectrometer. Upstream of the panel-1a arrays will be mounted the new panel-1b arrays. In the angular range from 35° to 45° will be the panel-2 arrays. These detectors were refurbished from the panel-2 arrays of the CLAS TOF system. A summary of the FTOF technical parameters is given in Table 1.

Fig. 2 shows the expected timing resolution as a function of counter length for the FTOF system. The magenta and blue curves indicate the design resolution for the panel-1a and panel-1b counters and the green curve indicates the design resolution for the panel-2 counters. The horizontal dashed line shows the nominal design average resolution in the forward direction of 80 ps used for the particle identification momentum limits discussed below.

Computing the flight time difference between different charged particle species as a function of momentum (see Fig. 3) shows that for an average time resolution of 80 ps, 4σ separation can be achieved between π/K up to 2.8 GeV, between K/p up to 4.8 GeV, and

Parameter	Design Value
Panel-1a	
Angular Coverage	$\theta = 5^\circ \rightarrow 35^\circ$, ϕ : 50% at $5^\circ \rightarrow$ 85% at 35°
Counter Dimensions	$L = 32.3$ cm $\rightarrow 376.1$ cm, $w \times h = 15$ cm $\times$ 5 cm
Scintillator Material	BC-408
PMTs	EMI 9954A, Philips XP2262
Design Resolution	90 ps $\rightarrow$ 160 ps
Panel-1b	
Angular Coverage	$\theta = 5^\circ \rightarrow 35^\circ$, ϕ : 50% at $5^\circ \rightarrow$ 85% at 35°
Counter Dimensions	$L = 17.3$ cm $\rightarrow 407.9$ cm, $w \times h = 6$ cm $\times$ 6 cm
Scintillator Material	BC-404 (#1 $\rightarrow$ #31), BC-408 (#32 $\rightarrow$ #62)
PMTs	Hamamatsu R9779
Design Resolution	60 ps $\rightarrow$ 110 ps
Panel-2	
Angular Coverage	$\theta = 35^\circ \rightarrow 45^\circ$, ϕ : 85% at $35^\circ \rightarrow$ 95% at 45°
Counter Dimensions	$L = 371.3$ cm $\rightarrow 426.1$ cm, $w \times h = 22$ cm $\times$ 5 cm
Scintillator Material	BC-408
PMTs	Photonis XP4312B, EMI 4312KB
Design Resolution	145 ps $\rightarrow$ 160 ps

Table 1: Table of parameters for the scintillators, PMTs, and counters for FTOF panel-1a, panel-1b, and panel-2 arrays.

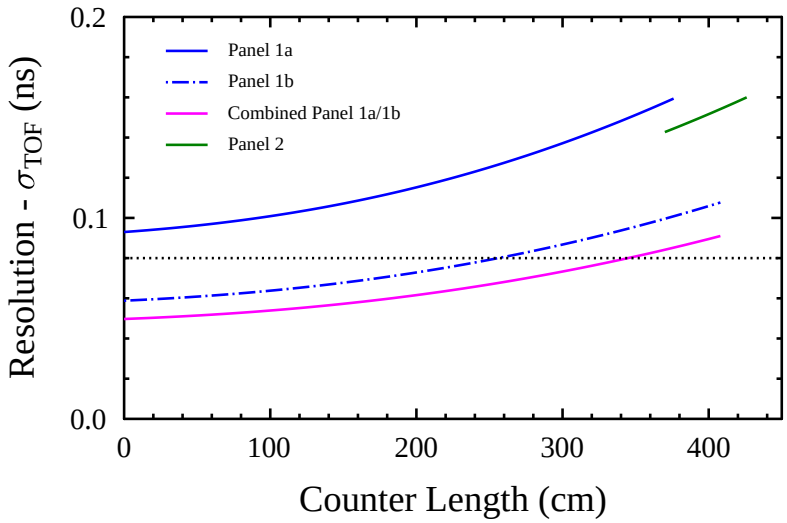

Figure 2: Design time resolutions for the FTOF panel-1a, panel-1b, and panel-2 counters as a function of the counter length. Also shown is the combined panel-1a and panel-1b time resolution curve.

between π/p up to 5.4 GeV. This 4σ threshold is a typical number that allows for hadron species separation with at least an order of magnitude difference in their yields.

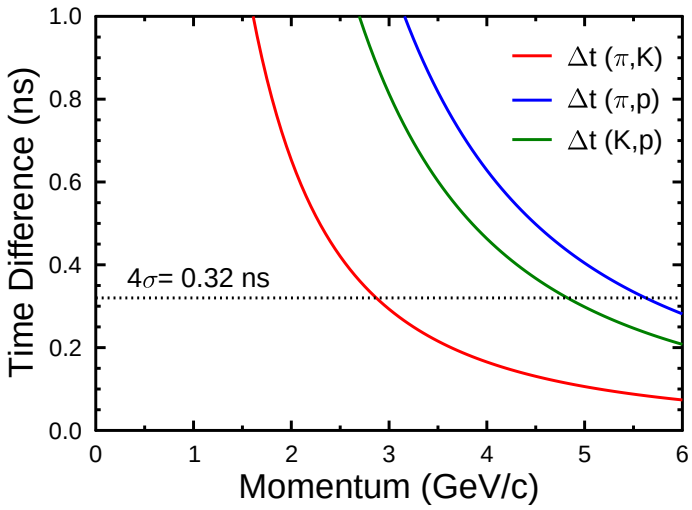

Figure 3: Time differences between pions and kaons (red), kaons and protons (green), and pions and protons (blue) over the 710 cm path length from the target to the FTOF system vs. momentum. The horizontal line indicates the 4σ separation time difference for the panel-1 counters.

2 FTOF Panel-1a and Panel-2 Refurbishment

The panel-1 TOF counter arrays were removed from the CLAS Forward Carriage on their support frames during August 2012. The panel-2 TOF counter arrays were removed from the CLAS North and South Clamshells in the period from August 2012 to January 2013. The panel-2 counters in S5 and S6 were removed attached to their associated support frames. The remaining counters were individually removed using special tooling. Fig. 4 shows photographs of the panel-1a and panel-2 removal from CLAS. All counters were placed on foam beds and cribbing and transported by truck to the FTOF refurbishment area in JLab Building 98.

The basic counter refurbishment steps involved the following procedures:

i). All counters were thoroughly cleaned using soft cotton rags dampened with a mild detergent.

ii). For the panel-1a arrays, the old (unused) centerline scintillator strips were removed from the face of the counters.

iii). A visual inspection of all counters was performed. Repairs of any light leaks found were made using electrical tape.

iv). The ends of the optical fibers that coupled to the laser calibration system were removed. For panel-1a, the fibers were cut at the base of the light-tight boot where they

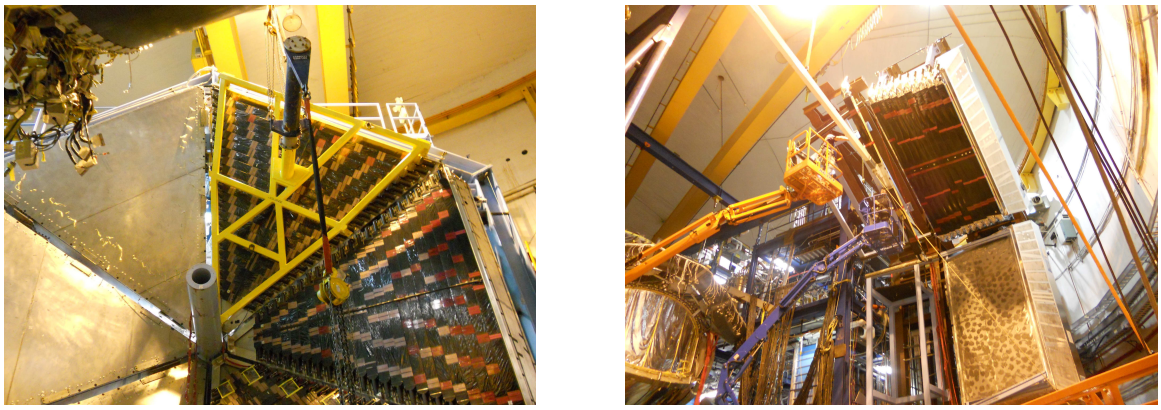

Figure 4: (Left) Photograph from August 2012 showing CLAS TOF panel-1 S3 being removed from the Forward Carriage. (Right) Photograph from October 2012 showing the CLAS TOF panel-2 S2 counters being removed from the South Clamshell.

entered into the scintillator wrapping. The holes were patched with a combination of light tight sealant [1] and electrical tape. For panel-2, the fibers ran along the outside of the counters in the gap between the underside of the counter and the backing structure. The fibers were cut at their entry point into the scintillator wrapping material. The insertion area was sealed with light tight sealant.

v). Any counters with broken light guide joints or broken PMT joints were opened up for inspection. For panel-1a, there were broken junctions between the small cylindrical light guide and the PMT face, as well as between the PMT and the small cylindrical light guide. For panel-2, several of the massive curved Acrylic light guides had become detached from the face of the scintillators.

- To access the junctions for panel-1a, the scintillator was unbolted from the frame and lifted out of the plane of the other counters. The electrical tape sealing the light tight boot (that contained the μ-metal shield) was removed and the voltage divider was unplugged. The light tight boot was then removed. Before re-gluing the light guides, any of the remaining glue was removed using ethanol as a solvent. Note that in all cases the cured glue film at the light guide/scintillator junction remained attached to the Acrylic light guide. If the light guide showed any cracks or scratches after inspection, it was sanded smooth by hand using a series of sandpaper grits starting at 1500 and going to 6000. If there were any deep gouges in the light guide, all rough edges were sanded until smooth. We then relied on the glue to fill any crevices when mating the light guide to the scintillator or to the PMT. For any broken PMT to light guide junctions, if the PMT did not have any evidence of cracks in the glass or loss of vacuum (seen by a clear environment when looking into the PMT glass), and if it was seen as a good PMT from the final CLAS baseline, the PMT was reattached to the light guide. The light tight boot and voltage divider were then re-attached and made light tight following the standard procedures.

- To access the junctions for panel-2, the electrical tape that holds the PVC tube con-

taining the μ-metal shield was removed and the shield tube and voltage divider were slid off over the PMT. A razor blade was then used to cut through both layers of the aluminized Mylar light tight boots in a 'T'-shape that allowed the boot to be opened up at the junction. Note that in all cases the cured glue film at the light guide/scintillator junction remained attached to the Acrylic light guide. After the light guide was removed by removing the two side attachment clamps, the surface of the light guide was cleaned with ethanol to remove the old glue. If the PMT attached to the light guide was found to be bad, either non-functioning or low gain, it was removed and replaced. At this point the standard procedures to seal the cut boot joints and reattach the shield tube were followed.

vi). Using the high voltage (HV) settings from the final CLAS TOF calibration determined in May 2012, the high voltage power supply was turned on. Using an oscilloscope, the average anode and dynode pulse heights and dark currents from each PMT were then recorded. Each PMT should have an average 1 V signal at the nominal PMT voltage and a dark current below 30 nA. Any PMTs that did not meet these requirements were flagged for further investigation.

- Channels that were noisy or had no signal were investigated again after replacing the associated voltage divider. If the voltage divider was good and there was no issue with connection to the PMT, the PMT was flagged for replacement if there was no evidence of a light leak in the counter.
- For panel-1a, any light tight boots that were cracked or chipped were repaired.
- Any PMTs with voltages above -2350 V were replaced if the divider checked good and there were no light leaks found in the counter. These PMTs fell into the low gain category.
- All scintillators were scanned with a light source to find any remaining light leaks. Any light leaks found were sealed with electrical tape.
- All new PMTs for panel-1a and panel-2 were tested for performance relative to a standard reference test PMT (an EMI 9954A for the 2-in PMTs and a Photonis XP4312B for the 3-in PMTs) before installation. All test results and data are contained in Ref. [2].

vii). After all repairs were made, the PMT signals (anode and dynode) were checked again with an oscilloscope and any other necessary repairs were made. All signal levels were recorded in the FTOF database [3].

viii). All panel-1a counters were realigned on their support frame. This includes left/right alignment to center them on their frames as well as along the counter to ensure they had the required clearance to the panel-1b mounting brackets. The attachment legs of the composite backing structures that were used to secure the counters to their frames were cut to accept the new panel-1b mounting brackets. The backing structures that were modified were associated with counters #5, #6, #14, #15, #18, #19, #22, and #23. Finally, the drilling template to

locate the panel-1b mounting brackets was aligned on each panel-1a frame and all required holes were drilled (see Fig. 5). The work procedures are defined by the steps in Refs. [4, 5]. After the drilling and alignment steps were completed, all counter signals were rechecked on the oscilloscope.

Figure 5: (Left) Photograph from October 2012 of the drilling template clamped into position on a panel-1a frame after alignment. The drill guides of the template control the pattern of holes drilled into the panel-1a frame. The eight panel-1b frame attachment pieces on each panel-1a frame (right) are attached using these holes.

ix). The panel-2 TOF arrays from CLAS consisted of 11 counters in each sector. For the FTOF panel-2 arrays, only five of these counters were employed. These included CLAS panel-2 counters #24, #26, #28, #30, and #32. These five counters were mounted on the new CLAS12 FTOF panel-2 frames (see Fig. 6) following the defined mounting and alignment procedures (see Ref. [6]). After mounting all counters, all PMT anode and dynode signals were checked on the oscilloscope.

Figure 6: Photograph taken in March 2013 during the mounting of the panel-2 S4 counters to their support frame.

Note: Due to differences in the frame mounting scheme for the panel-2 counters between CLAS TOF and CLAS12 FTOF, it was necessary for the existing definitions of the left and right ends of the counters to be swapped. Thus what is called the left (right) PMT for CLAS12 panel-2 was the right (left) PMT for CLAS panel-2.

x). The signal and HV cables were then installed on the panel-1a sectors on the underside of each frame in accordance with the overall FTOF cabling system design [7]. Fig. 7 shows how the cables were attached to the panel-1a frames on each side of the detectors using cable ties. The cable bundle must not extend past the bottom of the frame to have appropriate clearance with the PCAL windows. It also must be sufficiently far from the edge of the aluminum frame to allow for clearance to the brackets used to attach panel-1a to PCAL. All of the signal and HV cables for the FTOF system that connect from the PMTs to either the Forward Carriage electronics or the HV patch patches were labeled with both a human-readable label and a bar code label at each end prior to cable installation on the sectors. All cables were tested for continuity and shorts after they were labeled.

Notes:

- All PMTs and light guides were attached using UV curing glue, Dymax Ultra Light-weld adhesive, bonding UV-blocked acrylic and polycarbonate 3-20262 [8].
- Glue surfaces that required sanding were not polished to a mirror surface specifically to avoid problems with weak bond strength.
- When counter repairs required peeling back the wrapping about the ends and for those counters where both ends were open simultaneously, visual inspections of the scintillator quality with flashlights and lasers showed no evidence of scintillator discolorations. However, no quantitative radiometry checks were made. Also, spot checks of the aluminum foil layers showed no evidence that the foil had adhered to the scintillator surface near the ends of the bars.

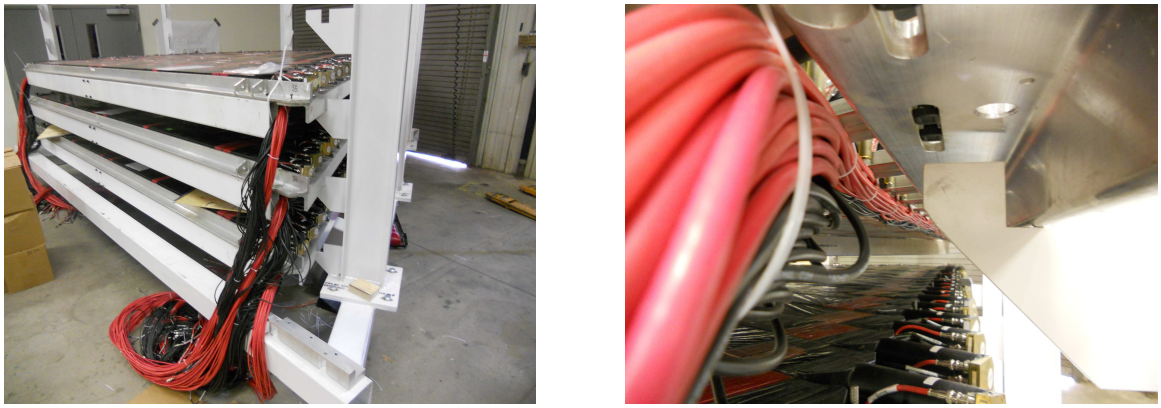

Figure 7: (Left) Photograph of the completed cabling on three of the panel-1a sectors from February 2013. (Right) Close up of the cabling attachment on the underside of one of the panel-1a sector frames.

Details on the counter refurbishment work in each sector are included in Tables 2 and 3 for panel-1a and in Table 4 for panel-2. As a summary of the work done, of the 276 PMTs in the panel-1a system (23 counters/sector $\times$ 6 sectors $\times$ 2 PMTs/counter), 45 PMTs were replaced and 15 light guides were re-attached. Of the 60 PMTs in the panel-2 system (5 counters/sector $\times$ 6 sectors $\times$ 2 PMTs/counter), 35 PMTs were replaced and 6 light guides were re-attached.

Paddle	Left Side	Right Side	Paddle	Left Side	Right Side
S1-01	New PMT		S2-01		Fixed LG
S1-02			S2-02		
S1-03	New PMT	Fixed LG	S2-03		
S1-04			S2-04		
S1-05			S2-05	Fixed LG	
S1-06			S2-06	New PMT	New PMT
S1-07			S2-07		
S1-08			S2-08		
S1-09			S2-09		
S1-10			S2-10		
S1-11			S2-11		
S1-12			S2-12		
S1-13			S2-13		
S1-14			S2-14		
S1-15			S2-15		
S1-16	New PMT		S2-16		New PMT
S1-17		New PMT	S2-17		
S1-18	Fixed LG		S2-18		New PMT
S1-19			S2-19		New PMT
S1-20			S2-20		
S1-21			S2-21		New PMT
S1-22		New PMT	S2-22		New PMT / Fixed LG
S1-23	New PMT	New PMT	S2-23	New PMT	New PMT
Paddle	Left Side	Right Side	Paddle	Left Side	Right Side
S3-01			S4-01	Fixed LG	Fixed LG & boot
S3-02			S4-02	Fixed LG	Fixed LG
S3-03			S4-03		
S3-04			S4-04		
S3-05	Fixed LG	Fixed LG	S4-05		
S3-06	Fixed LG		S4-06		
S3-07			S4-07		
S3-08			S4-08		
S3-09			S4-09		
S3-10			S4-10		
S3-11			S4-11	New PMT	
S3-12			S4-12		
S3-13			S4-13		
S3-14		New PMT	S4-14		
S3-15	New PMT		S4-15		
S3-16	New PMT	New PMT	S4-16		
S3-17			S4-17		New PMT
S3-18			S4-18		
S3-19	New PMT	New PMT	S4-19		New PMT
S3-20			S4-20		
S3-21			S4-21		New PMT
S3-22			S4-22		
S3-23	New PMT	New PMT	S4-23	New PMT / Fixed LG	New PMT

Table 2: PMT replacement and light guide repairs during refurbishment of the panel-1a S1, S2, S3, and S4 arrays.

Paddle	Left Side	Right Side	Paddle	Left Side	Right Side
S5-01			S6-01		
S5-02			S6-02		
S5-03			S6-03		New PMT
S5-04			S6-04		
S5-05			S6-05	New PMT	
S5-06			S6-06		
S5-07			S6-07		
S5-08			S6-08		
S5-09			S6-09		
S5-10			S6-10		
S5-11			S6-11		
S5-12		New PMT	S6-12		
S5-13			S6-13		Fixed LG
S5-14			S6-14		
S5-15		New PMT	S6-15		
S5-16			S6-16	New PMT	New PMT
S5-17	New PMT		S6-17	New PMT	
S5-18			S6-18		
S5-19			S6-19		
S5-20	New PMT		S6-20	New PMT	
S5-21			S6-21	New PMT	
S5-22	Fixed LG		S6-22		
S5-23	New PMT	New PMT	S6-23	New PMT	New PMT

Table 3: PMT replacement and light guide repairs during refurbishment of the panel-1a S5 and S6 arrays.

Paddle	Left Side	Right Side
S1-1	New PMT	
S1-2		New PMT
S1-3		New PMT
S1-4	New PMT	
S1-5	New PMT	New PMT
S2-1		New PMT
S2-2		
S2-3	New PMT	New PMT
S2-4	New PMT / Fix LG	
S2-5	New PMT	New PMT
S3-1	New PMT	New PMT
S3-2		
S3-3	New PMT / Fix LG	New PMT / Fix LG
S3-4		Fix LG
S3-5	New PMT / Fix LG	New PMT / Fix LG
S4-1	New PMT	New PMT
S4-2		
S4-3		
S4-4	New PMT	
S4-5		
S5-1	New PMT	New PMT
S5-2	New PMT	New PMT
S5-3		
S5-4	New PMT	New PMT
S5-5	New PMT	
S6-1		
S6-2	New PMT	New PMT
S6-3	New PMT	New PMT
S6-4	New PMT	
S6-5	New PMT	New PMT

Table 4: PMT replacement and light guide repairs during refurbishment of the panel-2 arrays.

3 DAQ Configuration and Triggers

For the FTOF HV calibrations and time resolution studies, the completed counter arrays were installed into storage carts. These carts were the basis of the FTOF cosmic ray test stand. The carts allowed for the individual scintillators of a given length or counter number in each sector to be aligned in vertical stacks. The panel-1a counters were installed in a separate set of carts than the panel-2 counters. Fig. 8 shows photographs of the different test stands. For the HV calibrations the individual counters were studied separately. However, for the time resolution studies, the bars of a given length or counter number for both panel-1a and panel-2 were studied in groups of three arrays at a time, called counter triplets.

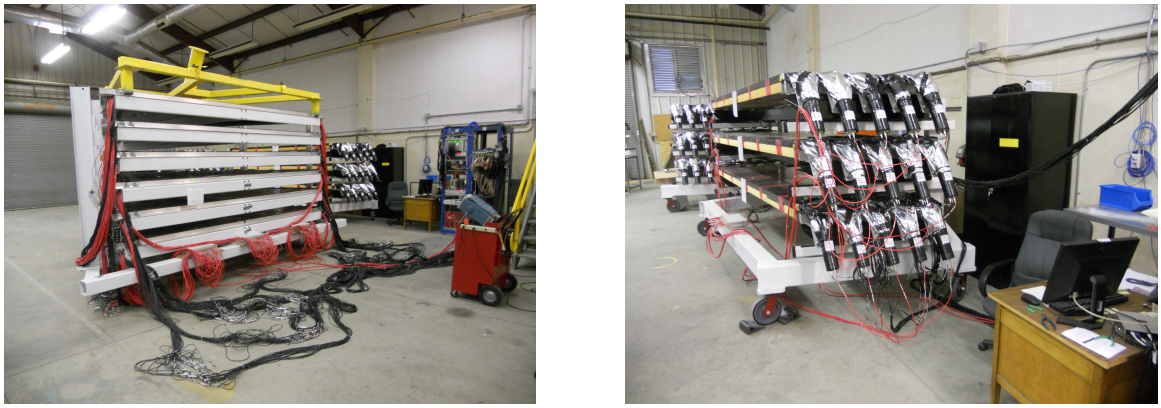

Figure 8: (Left) Photograph of FTOF panel-1a cosmic ray test stand. (Right) Photograph showing the two FTOF panel-2 triplets in their storage carts.

The analysis of each triplet proceeded first by completing a series of HV calibration runs to gain match the PMTs (runs 0.5 to 1 hr long) (see Section 4 for details). Then a long data run (≈6 hrs) was taken to study the average time resolution of each counter triplet (see Section 5 for details). Table 3 provides a summary of the data runs [9].

Triplet	Dates Studied	DAQ Runs	Long Run
Panel-1a: S1-S6-S5	4/1/13 - 4/24/13	146 - 166	166
Panel-1a: S2-S4-S3	4/24/13 - 5/9/13	171 - 225	218
Panel-2: S3-S4-S2	5/16/13 - 5/19/13	231 - 243	240
Panel-2: S5-S6-S1	5/20/13 - 5/21/13	245 - 251	251

Table 5: Summary of the time period of study and the associated runs taken for each panel-1a and panel-2 triplet configuration.

The DAQ system was setup as shown in Fig. 9 and included JLab 250 MHz VME flash ADCs into which the PMT dynodes were connected. It also included JLab VME discriminators and CAEN VME V1290a 35 ps LSB TDCs into which the anodes were connected. Fig. 10 shows a block diagram of the basic electronics configuration for each counter triplet. The standard run configuration included a trigger threshold of -50 mV and a TDC threshold of -20 mV (although other settings were studied). For the FADC, the integration window

was 400 ns long. The pedestal was measured for each event using an average of the first 30 samples. The signal was averaged from FADC samples 35 to 100.

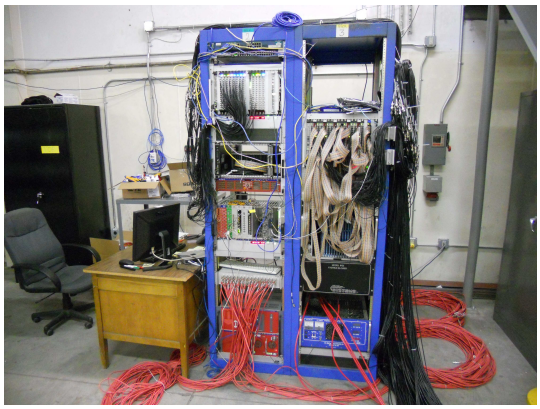

Figure 9: Photograph of the FTOF DAQ system including VME flash ADCs, discriminators, and high-resolution pipelined TDCs.

The trigger was defined by programming FPGAs located in the VME logic board (CAEN V1495). The data was acquired for each triplet employing two different trigger definitions:

$$\text{i). ``OR'' trigger: } \sum_{i=1}^{N} (\text{L} \cdot \text{R PMTs counter } i)_{layer\ 1} + \sum_{i=1}^{N} (\text{L} \cdot \text{R PMTs counter } i)_{layer\ 2} + \sum_{i=1}^{N} (\text{L} \cdot \text{R PMTs counter } i)_{layer\ 3}$$

$$\text{ii). ``Triplet'' trigger: } \sum_{i=1}^{N} \Big[(\text{L} \cdot \text{R PMTs counter } i)_{layer\ 1} \cdot (\text{L} \cdot \text{R PMTs counter } i)_{layer\ 2} \cdot (\text{L} \cdot \text{R PMTs counter } i)_{layer\ 3} \Big]$$

In these definitions the sum runs from $i = 1$ to N, where N is the number of triplets in the configuration. Thus N=23 for the panel-1a triplets and N=5 for the panel-2 triplets.

For the panel-1a triplet testing, initially the S1-S6-S5 triplet was in a separate storage cart from the S2-S4-S3 triplet. After QA testing was completed, the S1, S6, and S5 counter arrays were transferred to the cart containing S2, S4, and S3 (see Fig. 8). A full suite of data runs was re-taken to verify that the performance was unchanged after the detector movement.

4 HV Calibrations

The FTOF PMT high voltage settings were determined through dedicated calibration runs employing cosmic ray muons. The electronics trigger and the data analysis were set up to select those muons that went through the full extent of the counter from the front face to the back face. Fig. 11 shows different muon tracks passing through the scintillation bar. The ideal case of a normally incident muon passing through the face of the counter is shown in Fig. 11 (left). These minimum ionizing tracks deposit roughly 10 MeV as they pass through

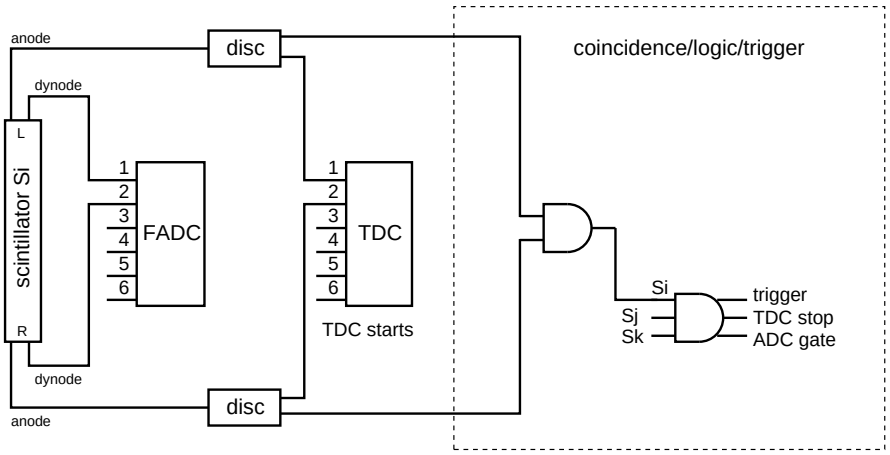

Figure 10: Block diagram of the electronics configuration for each triplet. The dashed line enclosed the trigger interface board.

the 5-cm thick FTOF panel-1a and panel-2 scintillation bars. (Remember that for minimum ionizing particles $dE/d\rho x = 2$ MeV/g/cm^2.)

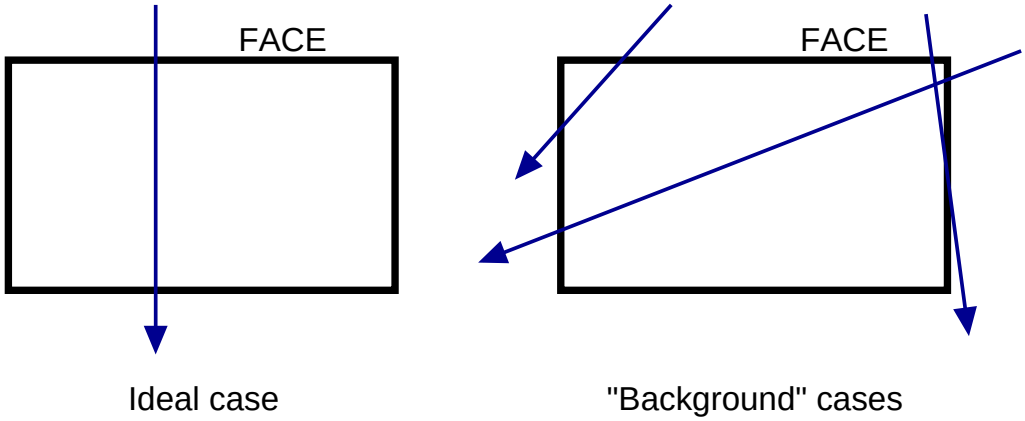

Figure 11: Representation of muon tracks passing through a scintillation bar. (left) Ideal case where the tracks are normally incident on the face of the bar. (right) Background events where the tracks clip the corners of the bar or pass through the side of the bars.

The energy deposited in the scintillator by the muons follows a Landau distribution. The ADC spectrum shows a peak above pedestal for the minimum ionizing muons from tracks close to the ideal case of Fig. 11 (left) as well as background events from tracks like those shown in Fig. 11 (right). The background events above the minimum ionizing peak arise from events with multiple track candidates, events from non-minimum-ionizing tracks, and events involving showers. The energy deposited is recorded by the ADC. For a given scintillation bar, the typical ADC spectrum appears as shown in Fig. 12. These events recorded in the ADC spectrum have been pedestal subtracted.

For the HV calibrations, to avoid issues with the attenuation of light for tracks that pass near the ends of the bars and to avoid issues with unbalanced light entering the left and right PMTs, we combine the information from the left and right PMTs to produce an average ADC spectrum for the counter through the quantity:

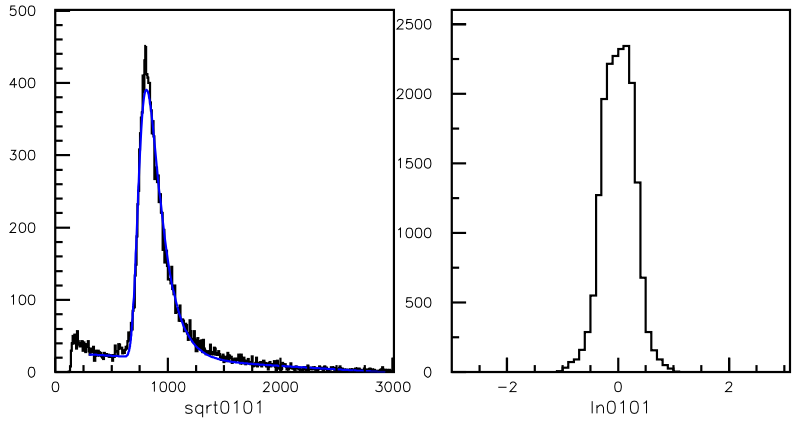

Figure 12: (Left) Average ADC spectrum ($\overline{ADC}$) and (right) log ratio spectrum (R) from a typical CLAS12 FTOF counter.

$$\overline{ADC} = \sqrt{(ADC_L - Ped_L) \cdot (ADC_R - Ped_R)}. \tag{1}$$

Given the finite dynamic range of the ADC, we have chosen to position the minimum ionizing muon peak in a particular ADC channel (Fig. 12 shows channel 800) so that it is safely above the pedestal, but leaves sufficient range for the more highly ionizing charged tracks of our typical physics events. The position of the muon peak in the ADC spectrum is set by the PMT HV setting.

It is well known that the PMT gains depend exponentially on the applied voltage. Expressed in a slightly different way, we can relate the PMT gain G_1 at a given voltage V_1 to the gain G_2 at a different voltage V_2 via:

$$\frac{G_1}{G_2} = \left(\frac{V_1}{V_2}\right)^{\alpha}. \tag{2}$$

This is a basic power law form with α representing the power law factor. For the FTOF PMTs, the typical value of α was determined to be between 7 and 14 depending on the PMT size and the trigger thresholds (see Section 4.2). Rewriting eq.(2) in a slightly different form, we have:

$$\frac{\Delta G}{G} = \alpha \frac{\Delta V}{V}. \tag{3}$$

It is this expression that is the basis for relating the average scintillator $\overline{ADC}$ setting (see eq.(1)) to the PMT HV setting. Eq.(3) tells us how much to increase or decrease the PMT HV settings to put the muon peak in the desired ADC channel.

Note that the gain-matching procedure then amounts to adjusting the HV settings of all PMTs to whatever values are required to position the muon peak for each counter in the desired ADC location. At the same time the algorithm uses the individual left and right ADC spectra for a given counter to ensure that the PMT gains are properly balanced.

4.1 HV Calibration Algorithm

This section details the algorithm for the basic HV calibration code for a given FTOF counter in a series of steps.

♢ **Step #1**:

Form the two basic calibration spectra for each counter. These are the average ADC spectra ($\overline{ADC}$) and the logarithmic ratio of the pedestal subtracted ADC data from the left and right PMTs of a given counter (R). Fig. 14 shows these sets of histograms for panel-1a S1 and Fig. 15 shows them for panel-2 S1.

$$\overline{ADC} = \sqrt{(ADC_L - Ped_L) \cdot (ADC_R - Ped_R)} \tag{4}$$

$$R = \ln\left[\frac{ADC_R - Ped_R}{ADC_L - Ped_L}\right]. \tag{5}$$

♢ **Step #2**:

(i). Fit the $\overline{ADC}$ spectrum to determine the centroid of the muon peak using a Landau function for the muon peak and a polynomial function for the background. Call this value $GAIN\_IN$. See the plots in Figs. 14 and 15 for fit examples.

(ii). Determine the statistical mean of the R spectrum. Call this value $CENTROID$.

♢ **Step #3**:

Determine the effective centroids of the left and right ADC distributions using the $GAIN\_IN$ and $CENTROID$ values from Step #2.

$$G_L = \frac{GAIN\_IN}{\sqrt{\exp(CENTROID)}}, \qquad \text{effectively } (ADC_L - Ped_L) \tag{6}$$

$$G_R = GAIN\_IN \cdot \sqrt{\exp(CENTROID)}, \qquad \text{effectively } (ADC_R - Ped_R). \tag{7}$$

♢ **Step #4**:

Compute the desired shifts in voltage using eq.(3).

$$\Delta G_{L,R} = 800.0 - G_{L,R}, \qquad \text{(to put muon peak in ADC channel 800)} \tag{8}$$

$$\Delta V_{L,R} = \frac{{V_{L,R}}^{ORIGINAL} \cdot \Delta G_{L,R}}{G_{L,R} \cdot \alpha}. \tag{9}$$

Thus $V_{L,R}^{NEW} = V_{L,R}^{ORIGINAL} + \Delta V_{L,R}$.

Notes:

- The PMT voltages should be negative, so the final settings from these values will actually be $-V_{L,R}^{NEW}$.

- The important step of determining the appropriate power law factor α is described in Section 4.2.

- The analysis of the data proceeded using PAW ntuples. As PAW does not have a built-in Landau function for fitting, an approximation to the Landau function was employed of the form:

$$\psi(\lambda) = \sqrt{\frac{e^{-(\lambda+e^{-\lambda})}}{2\pi}}, \tag{10}$$

  where $\lambda = width \times (ADC - centroid)$ [10].

4.2 Power Law Factor Determination

The determination of the power law factor α in eq.(2) is important in order to get the HV calibrations to converge in just a few iterations. Typically the factor of α is roughly equal to the number of dynode stages in the PMT. Both the 2-in and 3-in PMTs for panel-1a and panel-2, respectively, employ 12-stage PMTs. However, our direct measurements of α were on average 13.4 for panel-1a and 8.6 of panel-2. Note that because we are using the bipolar dynodes as input to the ADCs, it was found that α had a dependence on the integration range of the ADC. Also the values of α tended to show more fluctuations from PMT to PMT if there was any discernible noise on the signal baseline.

Regardless of the theoretical value of α, the best course for the HV calibrations is to measure this quantity directly. For this purpose two data runs were acquired with different HV settings for the PMTs. Them after determining the locations of the muon peaks from the ADC spectrum fits, eq.(3) was used to solve for α for all PMTs in the triplet configuration under study. The results of our measurements of α are shown in Fig. 13. For the panel-1a S1-S6-S5 triplet we measured an average value of α=13.4. For the panel-2 S3-S4-S2 triplet we measured an average value of α=8.6.

4.3 Results

The iterative process to determine the final set of PMT HV values typically converged in 3 to 4 data runs. The goal was to center the muon peak in the $\overline{ADC}$ spectrum for each counter in channel 800. In order to ensure that the left and right PMTs were well gain matched for each counter, the mean of the log ratio plot should be very close to zero, typically within the range from -0.02 to 0.02.

Representative final calibration spectra with the Landau and background fits are shown in Fig. 14 for panel-1a S1 and in Fig. 15 for panel-2 S1. The full set of average muon ADC peak centroids and log ratio centroids are shown for all panel-1a counters in Fig. 16 and for all panel-2 counters in Fig. 17. The HV values for each PMT are tabulated in Table 6 for panel-1a and in Table 7 for panel-2.

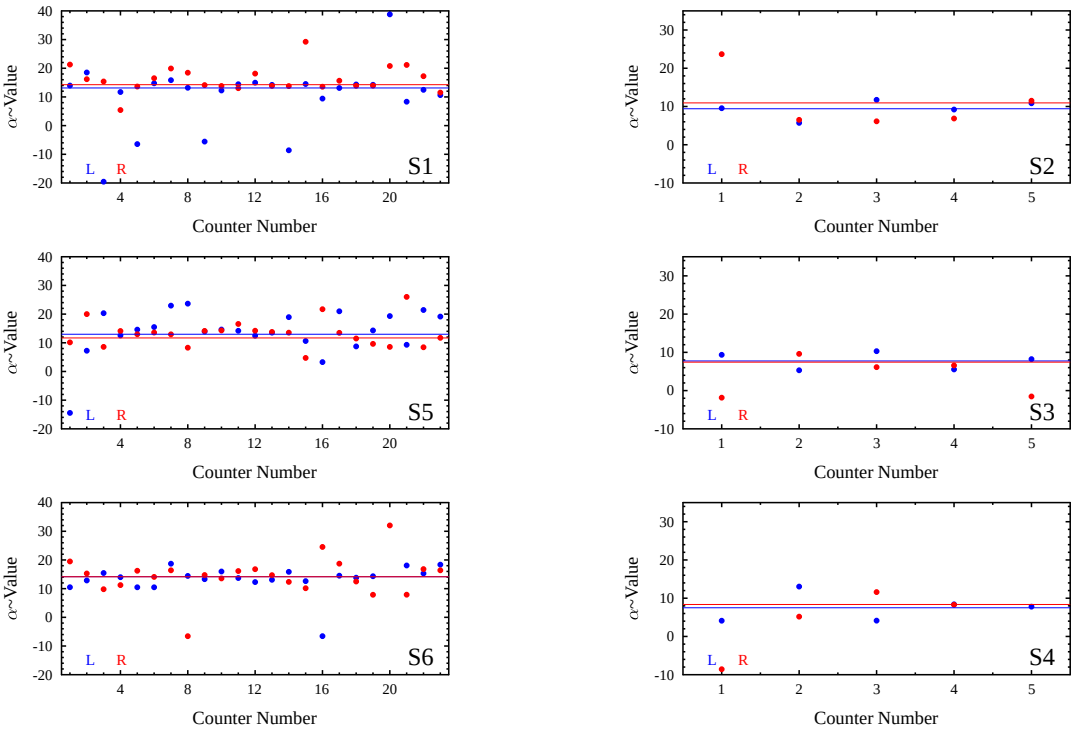

Figure 13: Data showing the measurement of the power law factor α for panel-1a (left) with $\langle\alpha\rangle$=13.4 and for panel-2 (right) with $\langle\alpha\rangle$=8.6.

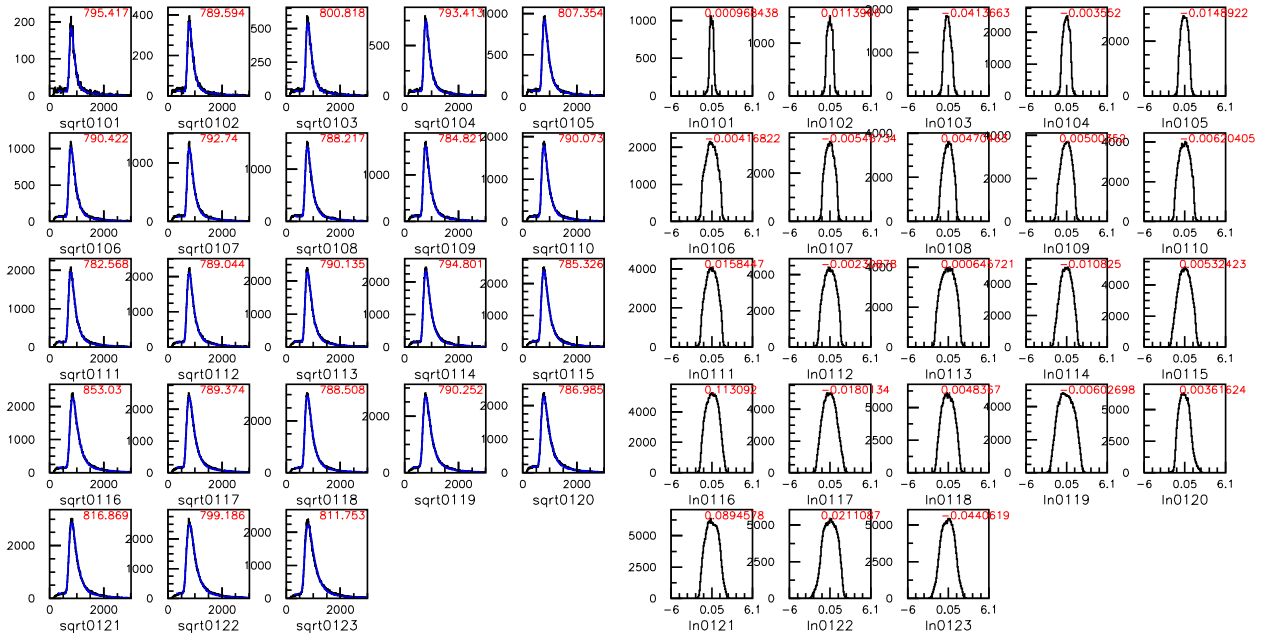

Figure 14: Panel-1a S1 - long run 166. (Left) Average ADC fits. (Right) Log ratio plots.

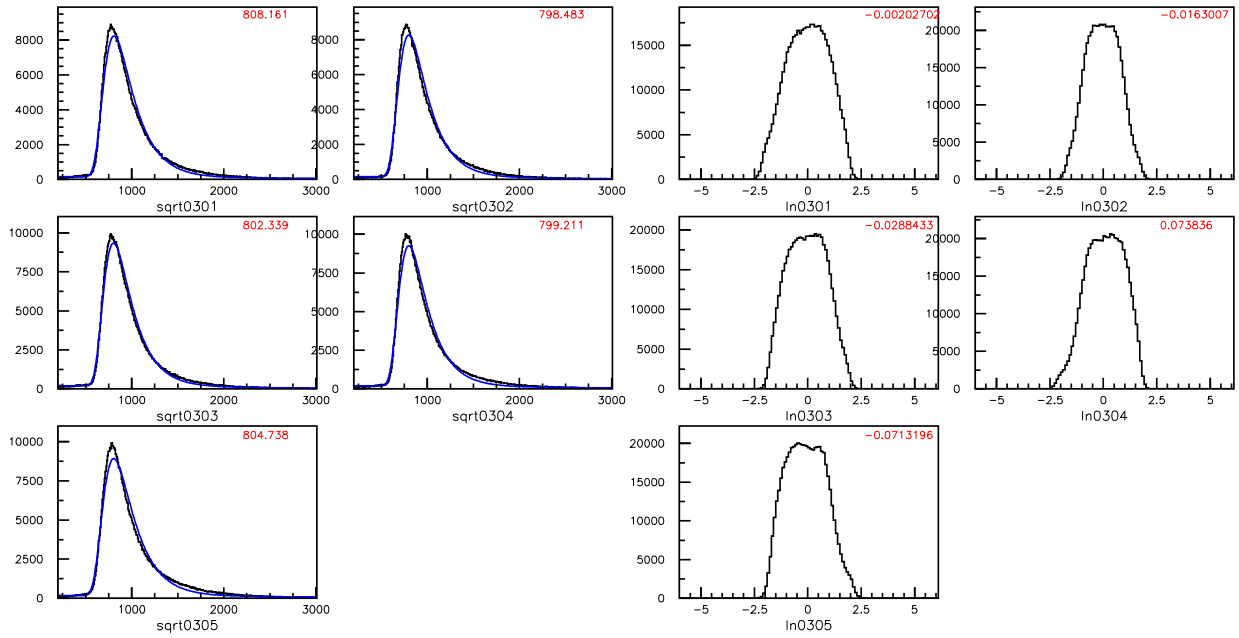

Figure 15: Panel-2 S1 - long run 251. (Left) Average ADC fits. (Right) Log ratio plots.

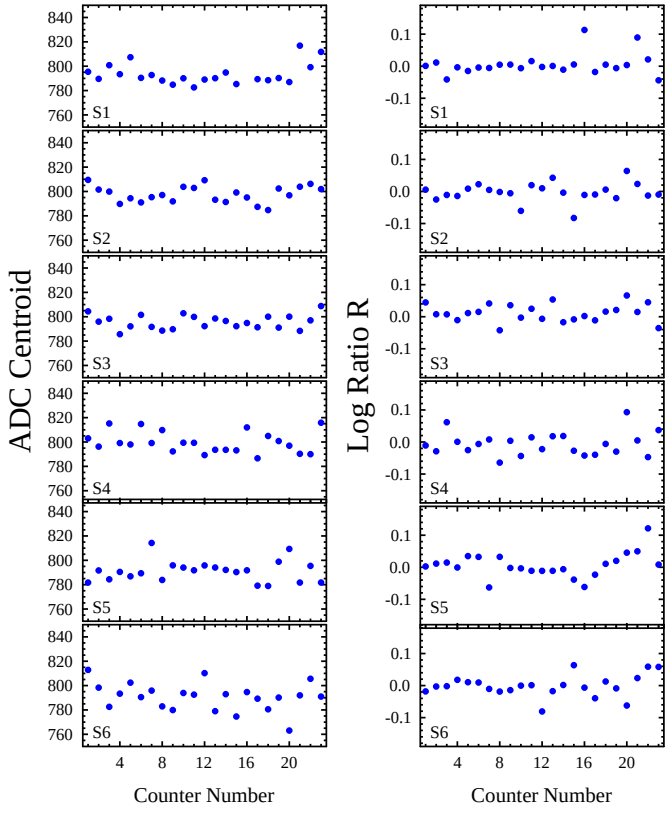

Figure 16: (Left) Values of the peak of the average muon ADC spectrum for each panel-1a counter. Nominally the HV settings were adjusted to set these to a value of 800. (Right) Statistical means of the log ratio plots to highlight the left/right PMT gain balancing for each panel-1a counter.

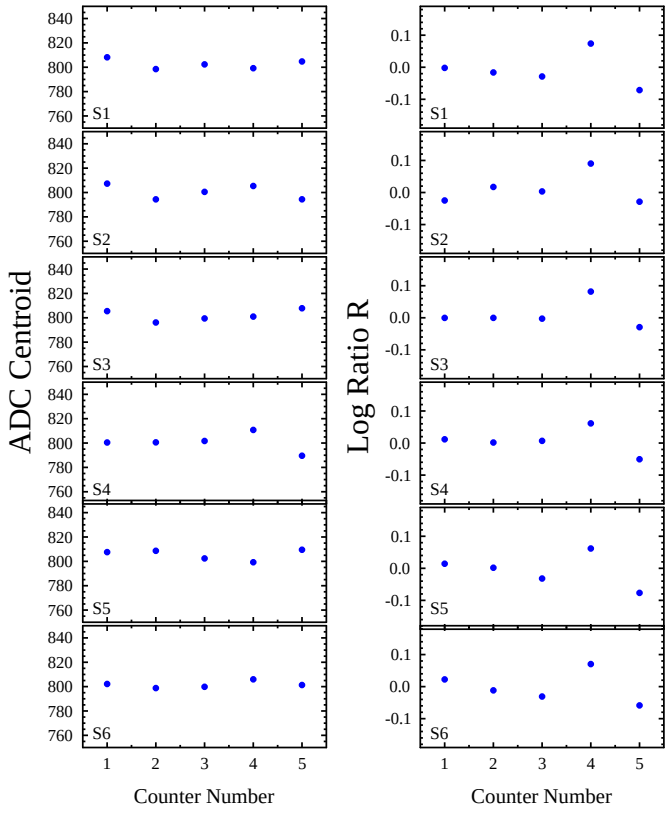

Figure 17: (Left) Values of the peak of the average muon ADC spectrum for each panel-1a counter. Nominally the HV settings were adjusted to set these to a value of 800. (Right) Statistical means of the log ratio plots to highlight the left/right PMT gain balancing for each panel-1a counter.

	S1		S2		S3		S4		S5		S6	
Counter	HV_L	HV_R	HV_L	HV_R	HV_L	HV_R	HV_L	HV_R	HV_L	HV_R	HV_L	HV_R
1	-1641	-1652	-1760	-1454	-1651	-1528	-1704	-1665	-1765	-1658	-1540	-1850
2	-1740	-1732	-1757	-1886	-1662	-1830	-1631	-1794	-1748	-1843	-1638	-1674
3	-1638	-1745	-1875	-1944	-1871	-1858	-1697	-1771	-1725	-1684	-1831	-1698
4	-1639	-1659	-2054	-1781	-1947	-1991	-1968	-1787	-1863	-1830	-1695	-1772
5	-1652	-1554	-1971	-1907	-1786	-1860	-1988	-1877	-1904	-1904	-1671	-1699
6	-1687	-1930	-1858	-1708	-1951	-2005	-1627	-1782	-1568	-1782	-1814	-1702
7	-1784	-1828	-1901	-1884	-1848	-2060	-1819	-1871	-1971	-1846	-1813	-1812
8	-1873	-1874	-1893	-1852	-2049	-2024	-2018	-1901	-1998	-1914	-1680	-1897
9	-2020	-1805	-2000	-1813	-1866	-1729	-1843	-1646	-1772	-1815	-1857	-2006
10	-1868	-2058	-1906	-1883	-1887	-1842	-1640	-1675	-1878	-1927	-1912	-1817
11	-1670	-2071	-1764	-1725	-2101	-1776	-1835	-1915	-1858	-1756	-1920	-1855
12	-1903	-2057	-1932	-2063	-1869	-2022	-1854	-1645	-1912	-1874	-2085	-1958
13	-2154	-1872	-1863	-1848	-1779	-1900	-2060	-2007	-1846	-2024	-1893	-1996
14	-1865	-1872	-1912	-2026	-1795	-1594	-2124	-1922	-2022	-2053	-2032	-1672
15	-2020	-2116	-2030	-2000	-1606	-2079	-1728	-2192	-1905	-1631	-2056	-1747
16	-1779	-1746	-1917	-1875	-1767	-1891	-1860	-1934	-1959	-1861	-1683	-1711
17	-2039	-1748	-1676	-1910	-2075	-1832	-2034	-1786	-1707	-1846	-1766	-2004
18	-1981	-2134	-1901	-1815	-1849	-1669	-1954	-1948	-1838	-2014	-1768	-1706
19	-2114	-1979	-1632	-1881	-1865	-1835	-1902	-1952	-1940	-1728	-1952	-2057
20	-1881	-2010	-1927	-2105	-1883	-2116	-1898	-2048	-1764	-1812	-1804	-2066
21	-1858	-1837	-2115	-1747	-2139	-1797	-1882	-1846	-1946	-1883	-1886	-1907
22	-1893	-1779	-1699	-1823	-2037	-1661	-1972	-2053	-2025	-1801	-1900	-1825
23	-1923	-1804	-2020	-1907	-1840	-1901	-1869	-1836	-1917	-1948	-1838	-1751

Table 6: Final gain-matched HV settings for the panel-1a counters after their refurbishment.

	S1		S2		S3		S4		S5		S6	
Counter	HV_L	HV_R	HV_L	HV_R	HV_L	HV_R	HV_L	HV_R	HV_L	HV_R	HV_L	HV_R
1	-1439	-1552	-1489	-1547	-1676	-1971	-1426	-1586	-1364	-1420	-1673	-1611
2	-1402	-1483	-1508	-1379	-1552	-1659	-1506	-1557	-1312	-1297	-1211	-1391
3	-1460	-1523	-1326	-1398	-1540	-1259	-2147	-1597	-1256	-1515	-1490	-1861
4	-1723	-1218	-1536	-1519	-1818	-1602	-1329	-1378	-1511	-1427	-1580	-1539
5	-1416	-1658	-1315	-1929	-1536	-1435	-1386	-1550	-1542	-1504	-1277	-1591

Table 7: Final gain-matched HV settings for the panel-2 counters after their refurbishment.

5 Time Resolution Measurements

During the initial assembly phase of the CLAS panel-1 and panel-2 TOF counters, detailed measurements of the timing resolution of each counter were completed using minimum ionizing cosmic ray muon tracks. From the CLAS technical publication on the TOF system [11], the measurements were presented as the average timing resolution for each counter of a given length vs. the counter length. This data is shown in Fig. 18. For the CLAS panel-1 counters, the average time resolution varied from ∼90 ps for counter #1 (32.3 cm long) to ∼140 ps for counter #23 (376.1 cm long). For panel-2, the average time resolution varied from ∼100 ps for counter #24 (371.3 cm long) to ∼140 ps for counter #34 (445.1 cm long).

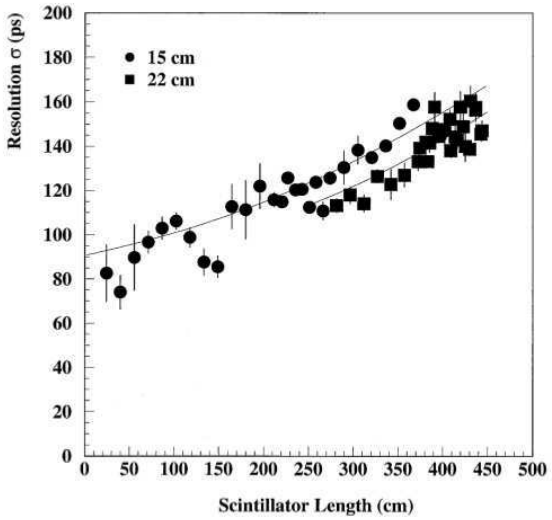

Figure 18: Measurement of the average TOF counter resolution of a given length counter (ps) vs. the counter length (cm). This data was acquired before the beginning of the CLAS production physics program and represents the initial baseline calibration [11].

As part of the QA procedure for the refurbished CLAS12 FTOF panel-1a and panel-2 counters, the average timing resolution of the different counters in each array was measured. The goal was to directly compare the new measurements to the baseline measurements of the same counters shown in Fig. 18.

The approach that was used for the timing measurements was to employ a "triplet" scheme. Here a set of three identical counters was used to measure the average timing resolution for the set. The basic configuration of the setup is illustrated in Fig. 19. For panel-1a 23 counter triplets were defined and for panel-2 5 counter triplets were defined. For these studies, the panel-1a triplets included the arrays S1-S6-S5 and S2-S4-S3. The panel-2 triplets included the arrays S3-S4-S2 and S5-S6-S1. In each of these listings, the first sector was on the bottom of the triplet stack and the last sector was on the top of the triplet stack.

5.1 Timing Resolution Algorithm

The basic algorithm to determine the average timing resolution of a set of three counters involves measuring the PMT timing for a given incident muon track. For a triplet measurement, where the track passes through all three counters with double-sided readout, six times are measured (t_1, t_2, ..., t_6). Each time measurement actually represents the difference

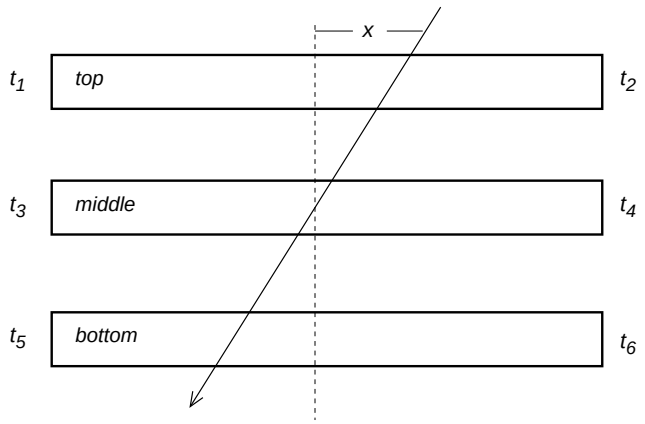

Figure 19: Schematic representation of a counter triplet made up of three identical scintillation counters. For the FTOF system, the scintillators have PMT readout at each end. The counters are labeled as top (t), middle (m), and bottom (b). The times t_i, $i = 1 \rightarrow 6$, represent the measured PMT times relative to the trigger time.

between the discriminated PMT signal (TDC start) and the trigger time (TDC stop from the six PMT coincidence). These timing measurements are then translated into three overall scintillation counter hit times:

$$\begin{aligned} t_t &= \frac{1}{2}(t_1 + t_2) \\ t_m &= \frac{1}{2}(t_3 + t_4) \\ t_b &= \frac{1}{2}(t_5 + t_6). \end{aligned} \tag{11}$$

Note that the coordinates of the hit along the counters can be determined through the time difference measurements of the PMTs via:

$$\begin{aligned} x_t &= \frac{v_{eff}}{2}(t_1 - t_2) \\ x_m &= \frac{v_{eff}}{2}(t_3 - t_4) \\ x_b &= \frac{v_{eff}}{2}(t_5 - t_6), \end{aligned} \tag{12}$$

where v_{eff} is the effective velocity of light in the scintillator material ($v_{eff} \approx 16$ cm/ns for BC-404 and BC-408).

For incident tracks that pass fully through each counter of the triplet with measured times t_t, t_m, and t_b, we can define a time residual t_r,

$$t_r = t_m - \frac{1}{2}(t_t + t_b). \tag{13}$$

We should expect that the time t_m of the middle scintillator hit should be the average of the measured times t_t and t_b for the top and bottom scintillator hits, respectively. Thus the

measured residual t_r should nominally be 0. However, due to the smearing of the measured times t_t, t_m, and t_b due to the finite time resolution of the measurements, the residual time t_r will also be smeared. While we still expect the mean of t_r to be zero, the width of the t_r distribution can be used to determine the average time resolution of each counter in the triplet.

The average time resolution of each counter is computed from the variance in the measured time residual. The time residual from eq.(13) can be rewritten as:

$$t_r = \frac{1}{2}(t_3 + t_4) - \frac{1}{2}\left[\frac{1}{2}(t_1 + t_2) + \frac{1}{2}(t_5 + t_6)\right], \tag{14}$$

therefore, the variance of t_r (written as δt_r) can be computed as:

$$(\delta t_r)^2 = \sum_{i=1}^{6}\left(\frac{\partial t_r}{\partial t_i}\right)^2 \Delta t_i^2 \tag{15}$$

$$= \frac{1}{16}\left(\Delta t_1^2 + \Delta t_2^2 + 4\Delta t_3^2 + 4\Delta t_4^2 + \Delta t_5^2 + \Delta t_6^2\right). \tag{16}$$

So,

$$\delta t_r = \frac{1}{4}\sqrt{(\Delta t_1^2 + \Delta t_2^2 + 4\Delta t_3^2 + 4\Delta t_4^2 + \Delta t_5^2 + \Delta t_6^2)}. \tag{17}$$

Assuming the average time resolution for each PMT in the triplet (Δt_i, $i = 1 \rightarrow 6$) is comparable, i.e. $\Delta t_1 = \Delta t_2 = \cdots = \Delta t_6$, then

$$\delta t_r = \frac{\sqrt{3}}{2}\Delta t_i = \frac{\sqrt{3}}{2}\sigma_{PMT}, \tag{18}$$

and we can write

$$\sigma_{PMT} = \frac{2}{\sqrt{3}}\delta t_r, \tag{19}$$

where σ_{PMT} is the timing resolution of the PMT. Given that each counter is readout using two PMTs, the overall counter timing resolution can be written as:

$$\sigma_{counter} = \frac{\sigma_{PMT}}{\sqrt{2}}. \tag{20}$$

Therefore we can write our final expression for the average counter timing resolution as:

$$\sigma_{counter} = \frac{2}{\sqrt{6}}\delta t_r. \tag{21}$$

Thus a measure of the width (σ) of the time residual distribution δt_r provides a measure of the average resolution of each counter in the triplet. Note that the exact form of the expression in eq.(21) depends on the specific formulation of the time residual definition in eq.(13).

Fig. 20 shows the time residual distribution from the S2-S4-S3 panel-1a triplet using the definition in eq.(13). Here the distribution of the hit coordinate vs. time residual is shown, as well as the projection onto the t_r axis. Fig. 21 shows the measured average triplet counter resolution from Gaussian fits to the residual distributions for the S2-S4-S3 panel-1a triplet before any time-walk corrections to the data.

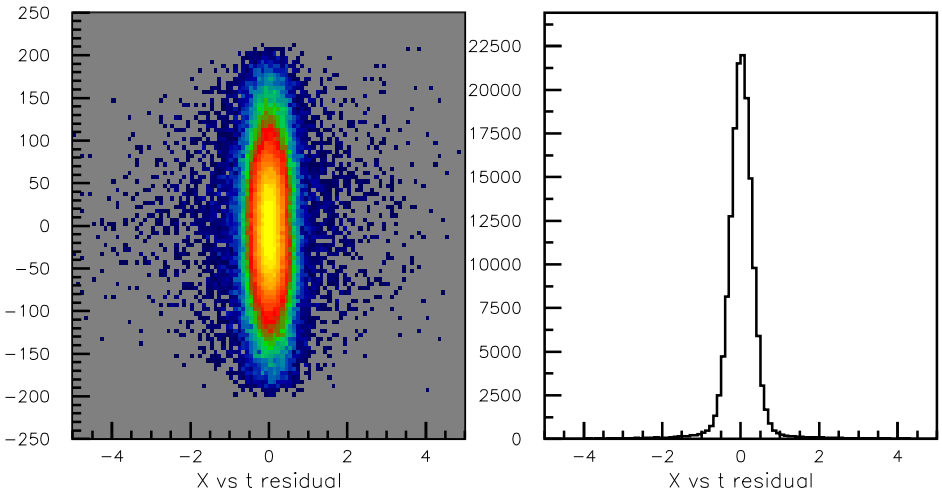

Figure 20: Data from the S2-S4-S3 panel-1a triplet for counter #23. (Left) Plot of the triplet hit coordinate (cm) vs. the time residual t_r (ns). (Right) The triplet time residual distribution (ns).

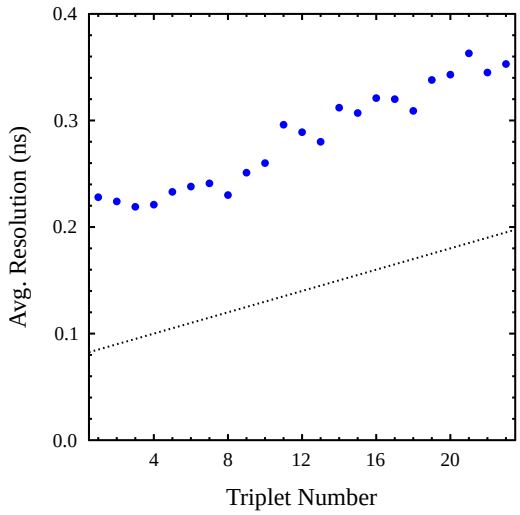

Figure 21: Fit of the residual distribution to determine the average triplet time resolution for each of the 23 counters from the S2-S4-S3 panel-1a triplet. The dashed line represents the average panel-1a counter time resolution from the initial baseline calibration for the CLAS TOF counters shown in Fig. 18. No time-walk corrections have been applied to these data.

5.2 Time Walk Corrections

During the standard TOF system timing calibrations for physics runs, one of the important corrections necessary to achieve precise timing resolutions is what is called a "time-walk" correction. Time walk is an instrumental shift in the measured hit time that arises when using leading edge discriminators [12]. This shift in timing arises due to the finite rise time of the analog pulse. For a given event time, pulses of different amplitude cross the discriminator threshold at slightly different times. This correction therefore depends on the ADC pulse size. Fig. 22 shows an example of the size of the correction for the panel-2 counters. Here the time residual from eq.(13) is plotted vs. the ADC value. In fact, all data for t_r^L vs. ADC^L and t_r^R vs. ADC^R for all counters in the panel-2 triplet are included in this same plot. These data show that the time walk correction is very similar for all panel-2 counters. In fact, the correction was founded to be the same for all panel-2 and panel-1a counters.

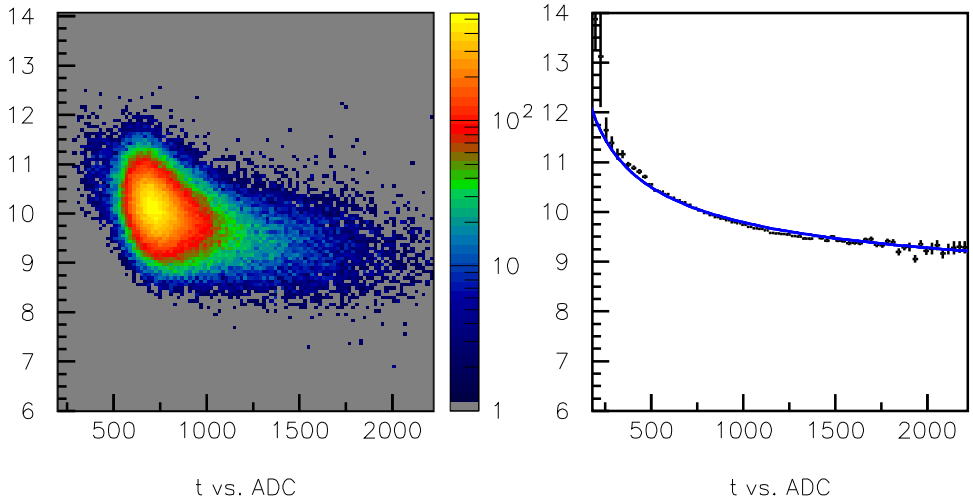

Figure 22: Plot of the measured TDC time for the middle counter of the panel-2 triplet relative to the average time of the outer layers of the triplet (the time residual of eq.(13)) (ns) vs. ADC pulse height, showing the importance of time walk corrections to optimize the timing resolution. The plot on the right is the same as that on the left but shows the average t_r with statistical uncertainty vs. ADC. These data were plotted with a cut on the reconstructed coordinate along each bar of the triplets to be with ± 10 cm of the middle of the counters.

Note that for the minimum ionizing muon tracks that have been positioned in the ADC spectra at channel 800 during the HV calibration (see Section 5.1), the cosmic ray data populate the precise region of phase space where the time walk corrections have the largest gradient. Over the full dynamic range of the ADC, the corrections are at the level of 3 ns. Keep in mind that the desired time resolution (see Fig. 18) is ultimately required to be at the level of about 100 ps.

In the range of the cosmic ray data, a very good representation of the time walk correction function is provided by the form [13]:

$$t_{walk}^{L,R} = \frac{A_0}{1 + A_1\sqrt{ADC^{L,R}}}, \quad \text{with } A_0 = 50.0, A_1 = 0.852. \tag{22}$$

Here, ADC is the pedestal-subtracted ADC value for each PMT.

5.3 Results

Correcting all measured times $t^{L,R}$ with the time walk correction function of eq.(22) for all panel-1a and panel-2 counters, the final average time resolutions for each triplet for panel-1a and panel-2 are shown in Fig. 23. The average time resolutions for the counters in the panel-1a S1-S6-S5 and S2-S4-S3 triplets were found to be slightly better (∼15%) than that achieved for the baseline measurements. For panel-2, the average time resolution was found to be slightly worse (∼15%) than the baseline measurements.

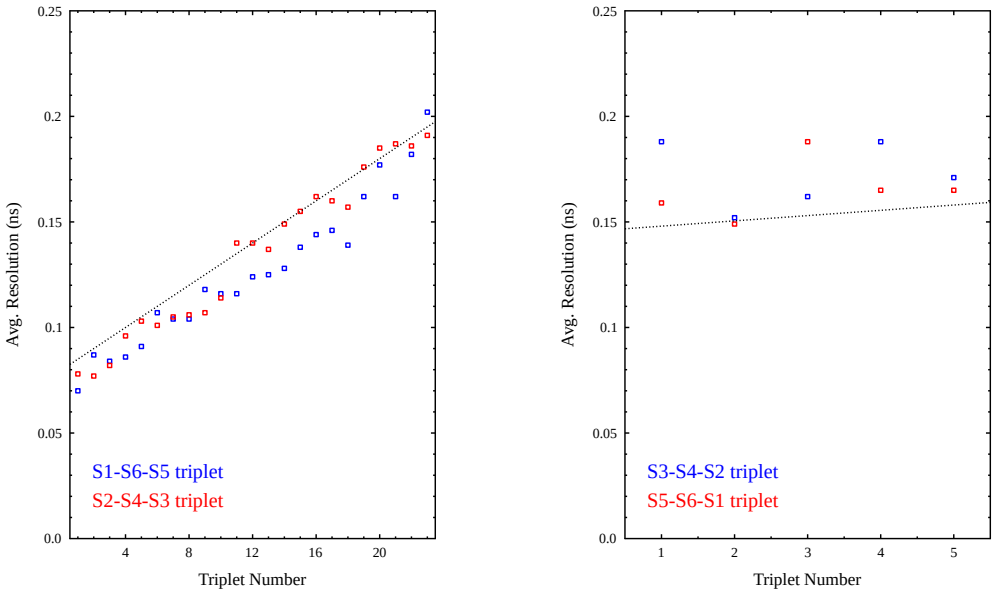

Figure 23: Final average triplet time resolutions for the refurbished FTOF panel-1a (left) and panel-2 (right) counters. The dashed line represents the average panel-1a counter time resolution from the initial baseline calibration for the CLAS TOF counters shown in Fig. 18.

In order to measure the average counter time resolutions for each counter, a number of corrections and cuts on the data were essential. These included:

1). The centroid of the left/right time difference $\Delta t = t_L - t_R$ for each counter was measured and added as a time offset to t_L to center the time difference distributions about zero. Note that $\langle \Delta t \rangle$ can be shifted from zero even with matched cable lengths on both PMTs due to differences in transit time of the PMTs. These time difference centroids were typically within ±2 ns (see Fig. 24 (left)). However, for several of the panel-2 counters, time differences up to 14 ns were seen.

After the Δt distributions for each counter were centered about zero, eqs.(12) could be used to determine the hit coordinates along each bar. Fig. 25 shows the hit coordinates from one of the sectors in the panel-1a studies. Note that the coordinate distributions are not uniformly populated for the longest bars at the ends due to light attenuation effects and due to the choice of electronics thresholds.

2). Once the $\Delta t_{L,R}$ distribution for each counter was shifted to be centered at zero, the time residuals for each triplet could be computed using eq.(13). These distributions too can have slight shifts from zero due to the same issues that caused $\Delta t_{L,R}$ to be shifted from zero.

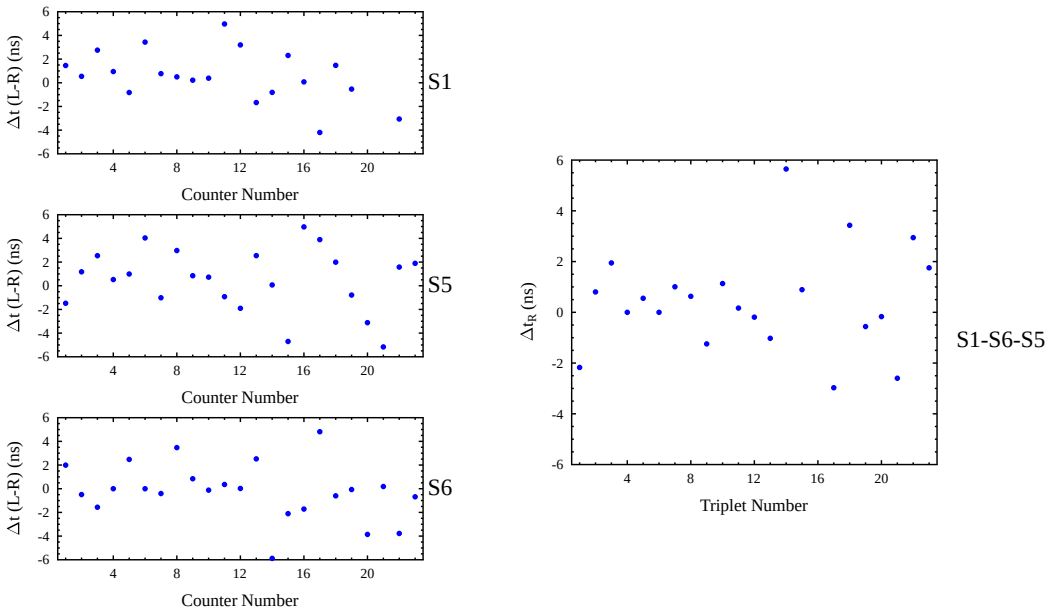

Figure 24: (Left) Distribution of the measured left/right time offsets for the panel-1a S1-S6-S5 triplet (ns) vs. counter number. (Right) Distribution of the triplet residual time offsets for the panel-1a S1-S6-S5 triplet (ns).

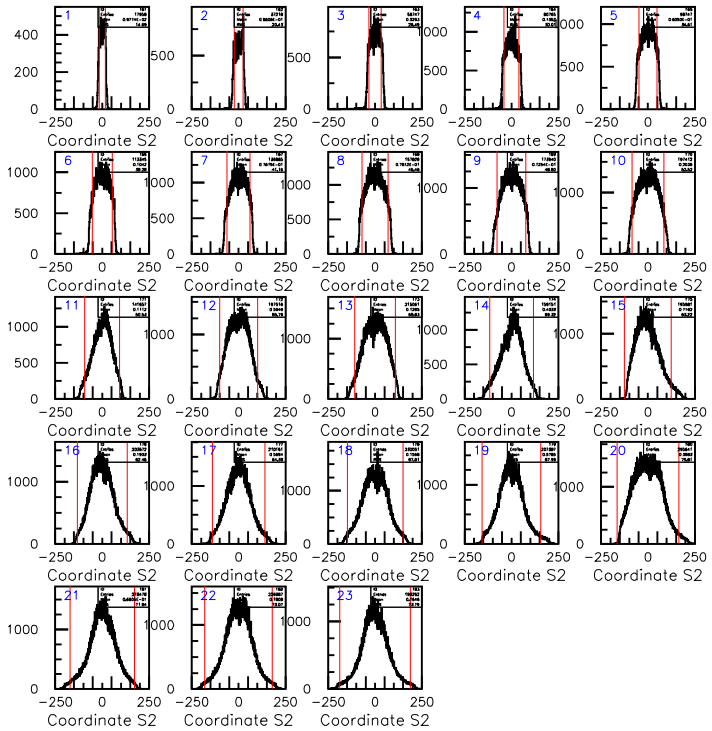

Figure 25: Reconstructed hit coordinates (cm) from the data for panel-1a S1 after the average left/right time offsets for each counters were shifted to zero. The red vertical lines indicate the nominal extent of each counter.

Thus the next step in the analysis was to determine all time shifts necessary to center the t_r distributions for each triplet to be centered at zero. One set of these offsets is shown for a panel-1a triplet in Fig. 24 (right).

3). With the hit coordinates along the bars reconstructed, the average time resolution vs. coordinate can be measured as shown in Fig. 26. The coordinate used here is that from the middle bar of the triplet. Note that the resolution is best near the center of the counter and reasonably flat over the coordinate range between -80 cm and 80 cm. Near the ends of the bars, the resolution gradually becomes worse due to light loss from to attenuation effects associated with the PMT farthest from the hit.

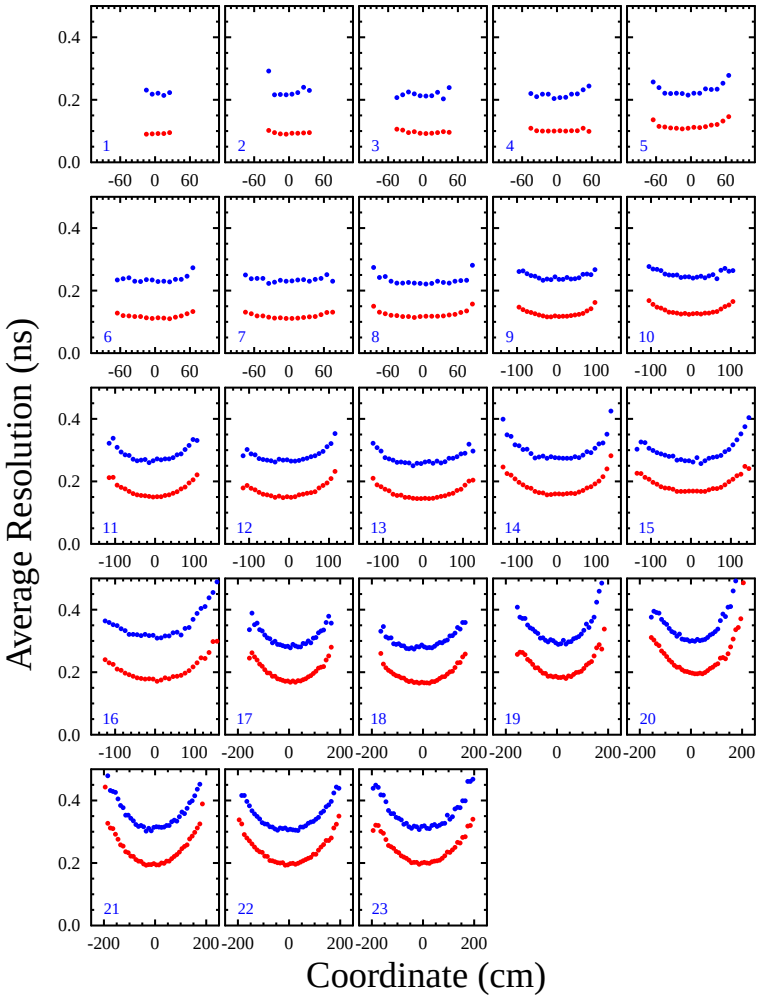

Figure 26: Average time resolution vs. coordinate for each of the counters in the S1-S6-S5 panel-1a triplet. The blue data points are before the time-walk correction and the red data points are after the time-walk correction.

4). Given the reconstructed coordinates, the angle of the incident muon tracks can be computed knowing the separation between the layers of the triplet arrays. The incident track angle relative to the normal to the plane of the counters is computed from the hit coordinates as:

$$\theta = \text{atan}\left(\frac{coor_{layer\ i} - coor_{layer\ j}}{D}\right), \tag{23}$$

where D is the separation between layer i and layer j. Fig. 27 shows the reconstructed angle from using the outermost layers of the triplet, which gives the most accurate angle determination. Fig. 27 also shows the correlation between the angle computed using different layers of the triplet.

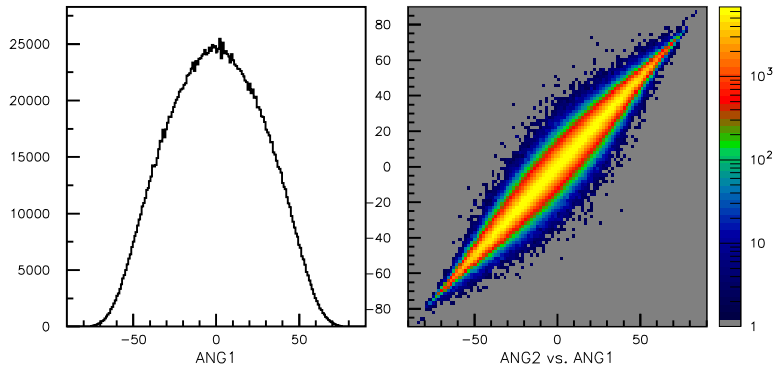

Figure 27: Analysis of panel-1a S2-S4-S3 triplet summing over all triplet sets. (Left) The angle of incidence of the muon tracks using the outermost layers of the triplet to compute the angle. (Right) Comparison of the angle computed using the outermost layers of the triplet to that computed using the top two layers of the triplet. (Angles measured in deg.)

Fig. 28 shows the resolution as a function of the angle of incidence of the muon track. These data show that the resolution is relatively independent of angle even before the time walk corrections. Near the angle acceptance extrema ($|\theta| > 60°$) the average triplet time resolution gets a little better as more light is created by the passing muons for the longer path lengths through the bars.

5). The time resolution also depends on the average ADC values as shown in Fig. 29. For optimal resolution, the very low ADC values, where the muon does not pass through the full extent of the counters, or very high ADC values, where the contributions are due to showering events, need to be cut out. Fig. 29 shows that the average triplet time resolution before the time-walk corrections is best right around the minimum ionizing events. It then quickly gets worse for increasing ADC values. This clearly shows that although higher ADC values imply more light collected, that the time-walk effects dominate the resolution. After making the time-walk corrections, the resolution vs. average ADC value is relatively flat up to an average ADC value of about 2000. It then gets worse for higher ADC values. This is due to the fact that the time-walk correction form employed here (see eq.(22)) was optimized for the range of these cosmic data. Other functional forms that better describe the data for a broader ADC range will be required for the optimization of the time resolution for physics data.

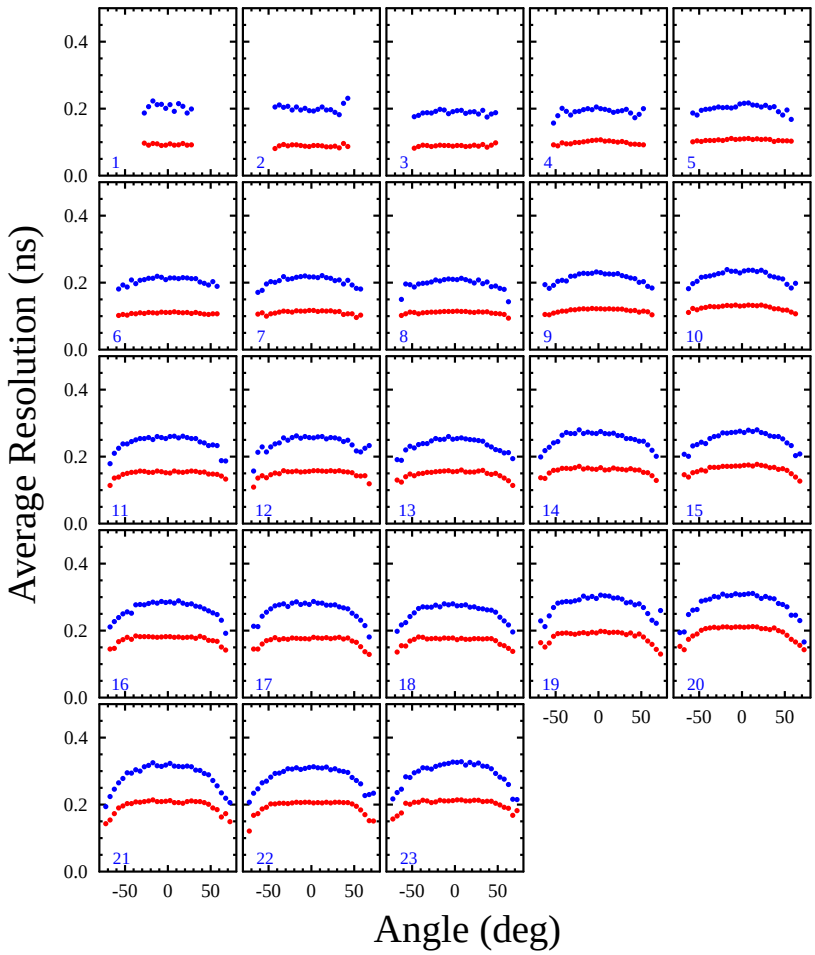

Figure 28: Average time resolution vs. track incident angle for each of the counters in the S1-S6-S5 panel-1a triplet. The blue data points are before the time-walk correction and the red data points are after the time-walk correction.

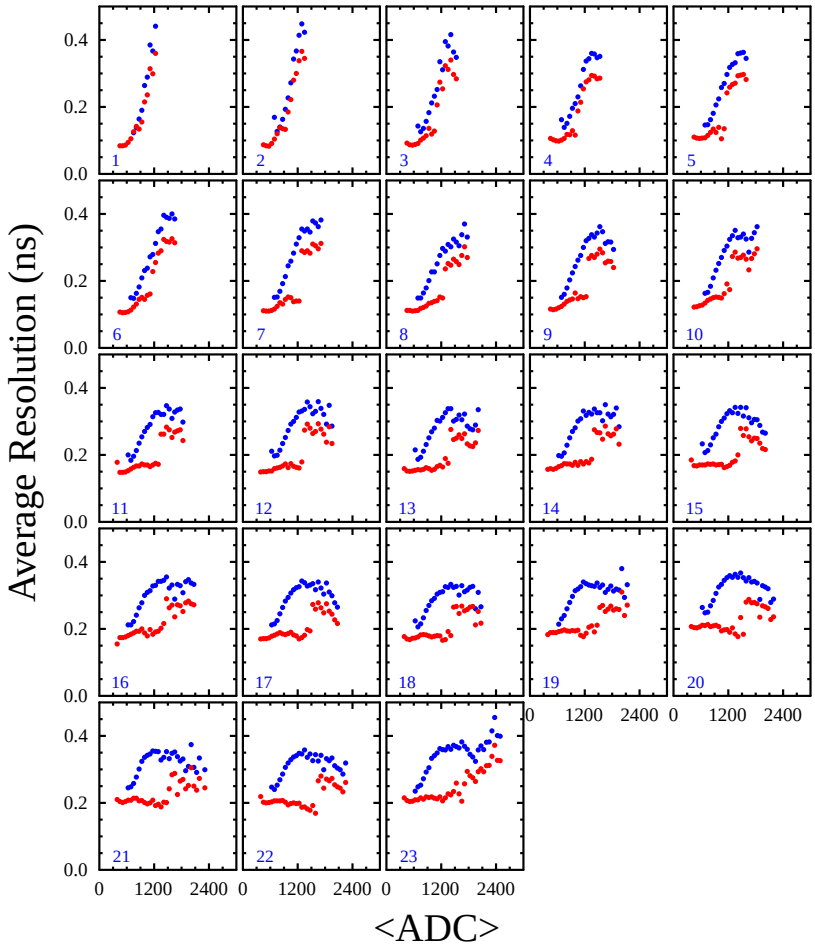

Figure 29: Average time resolution vs. average ADC value for each of the counters in the S1-S6-S5 panel-1a triplet. The blue data points are before the time-walk correction and the red data points are after the time-walk correction.

For the final analysis results shown in Fig. 23, the following cuts have been applied:

1. Triplet trigger - requires good TDC time for all 6 PMTs in a given triplet.
2. $\theta_{top/bottom} \leq \pm 20^{\circ}$ and that all 3 pairs of counters give a consistent angle measure.
3. $0.9 \cdot \overline{ADC}_C < \overline{ADC} < 1.4 \cdot \overline{ADC}_C$ for all counters in a given triplet, where $\overline{ADC}_C$ is the peak of the muon distribution in the average ADC spectrum.
4. x-coordinate within ± 80 cm.
5. Time-walk correction.

6 Attenuation Length Measurements

The attenuation length of the scintillator bars represents the distance λ into the material where the probability that the photon has been absorbed is $1/e$. For the scintillator bars, as more light collected translates into better timing resolution, it is important for the attenuation length to be as long as possible. For scintillators, it is generally hoped that the attenuation length is at least on the order of the overall length of the bars.

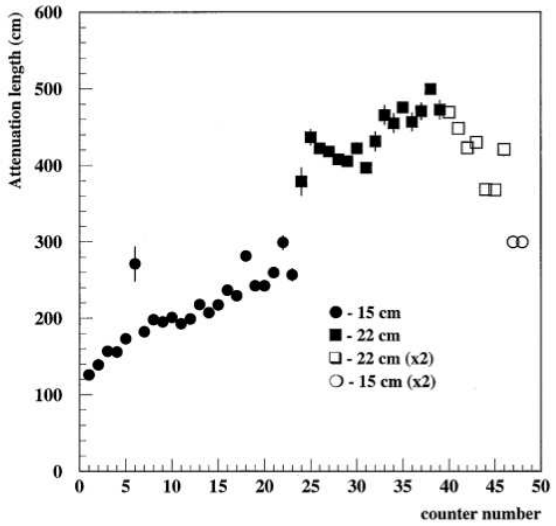

Figure 30: Baseline data from the CLAS TOF NIM paper [11] for the attenuation lengths of the counters vs. counter number.

For scintillation counters there are actually two attenuation lengths that are talked about. The first is the attenuation length for the bulk material. For BC-408, this bulk attenuation length is reported by the manufacturer as 380 cm [14]. However, the effective attenuation length for a finite geometry bar of the scintillation material is considerably shorter to the reflections at the surfaces of the bar (and inherently dependent on the specific geometry of the bar). Therefore, the true practical attenuation length of the material turns out to be about half the bulk attenuation length. The extracted values from the refurbished FTOF panel-1a and panel-2 counters can be compared against the baseline data from the CLAS TOF NIM paper [11] shown in Fig. 30.

The probability of finding a photon at a depth x into the material is calculated using:

$$P(x) = e^{-x/\lambda}. \tag{24}$$

This can be rewritten in terms of the measured ADC values for the left and right PMTs of a given counter as:

$$\begin{aligned} A^L &= A_0^L e^{+x/\lambda_L} \\ A^R &= A_0^R e^{-x/\lambda_R}, \end{aligned} \tag{25}$$

where A_0^L and A_0^R are constants and λ_L and λ_R are the left and right counter attenuation lengths. Then,

$$\ln\left(\frac{A_L}{A_R}\right) = \mathcal{C} + \frac{2x}{\lambda}, \quad \text{assuming } \lambda_L = \lambda_R = \lambda. \tag{26}$$

This is a linear form with y-intercept $= \mathcal{C}$ (a constant) and slope $= 2/\lambda$. Thus a linear fit of the log ratio of A_L/A_R vs. coordinate can be used to extract the effective counter attenuation length. Fig. 31 shows a sample of the fits of the log ratio plots to determine the counter attenuation lengths. Fig. 32 shows the measured average attenuation lengths for the panel-1a and panel-2 counters.

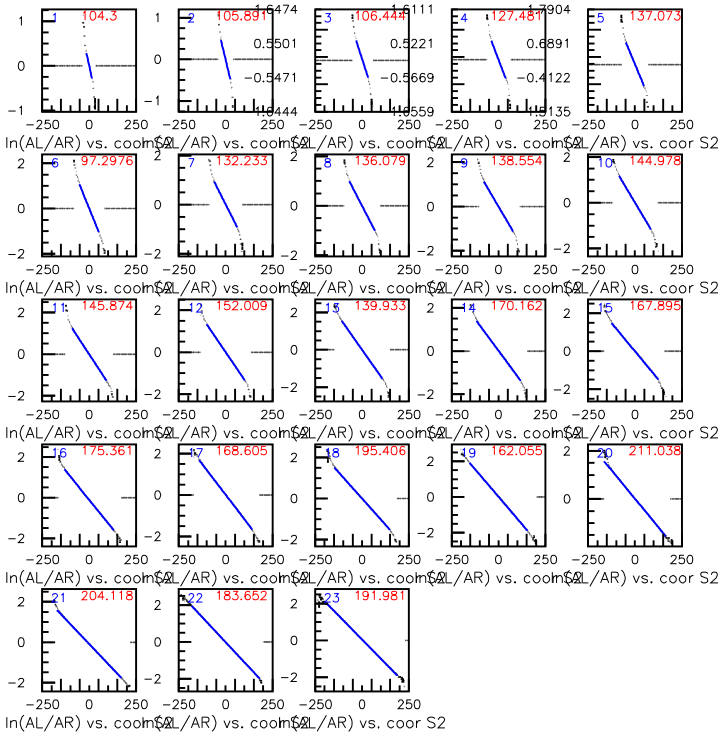

Figure 31: Plots of the ADC left/right log ratio vs. coordinate (cm) for panel-1a S2. The blue lines are the linear fits to these distributions as in eq.(26).

The attenuation lengths measured for panel-1a are seen to be ∼20% shorter than for the baseline from Fig. 30. For panel-2 the measured data are curiously seen to be a factor of two shorter than for the baseline data. However, the panel-1a and panel-2 attenuation lengths

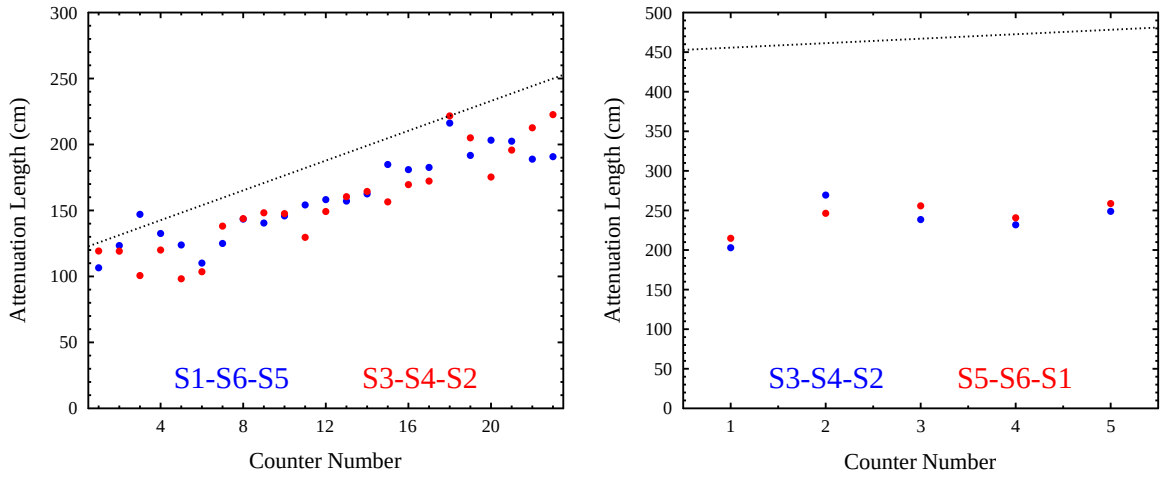

Figure 32: Measured average attenuation lengths for the panel-1a triplets (left) and the panel-2 triplets (right). The dashed lines on each figure are the baseline expectations from Fig. 30.

from the refurbished counters show clear consistency vs. the counter length as shown in Fig. 33.

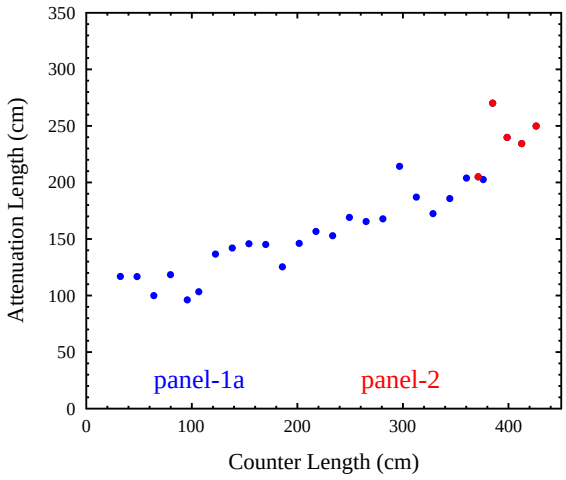

Figure 33: Average counter attenuation length for all FTOF panel-1a counters (blue points) and panel-2 counters (red points) as a function of counter length.

Note that the λ measurement for a panel-2 counter of the same length as a panel-1a counter is expected to be slightly longer than for panel-1a due to the slightly wider bar geometry relative to panel-1a (22 cm width for panel-2 vs. 15 cm width for panel-1a). This allows for a larger acceptance for direct light. The baseline data for panel-2 clearly does not make sense as the measured attenuation lengths in Fig. 30 are unphysically longer than the bulk attenuation length for the material. Thus the comparisons between the old baseline results from the CLAS TOF NIM paper [11] and the refurbished FTOF panel-1a and panel-2 counters for the attenuation length should not be taken too far and certainly cannot be used to ascertain the current relative quality (i.e. transparency) of the material.

Next we can determine the hit coordinates using the measured ADC values and the extracted attenuation lengths. Using the expressions in eq.(25), we can solve for the coordinate

as:

$$coor = \frac{\lambda}{2} \ln\left(\frac{A_L}{A_R}\right), \quad \text{assuming } \lambda_L = \lambda_R = \lambda. \tag{27}$$

Note that Fig. 34 shows the coordinates from the measured ADC pulse heights agree well with those from the TDC information.

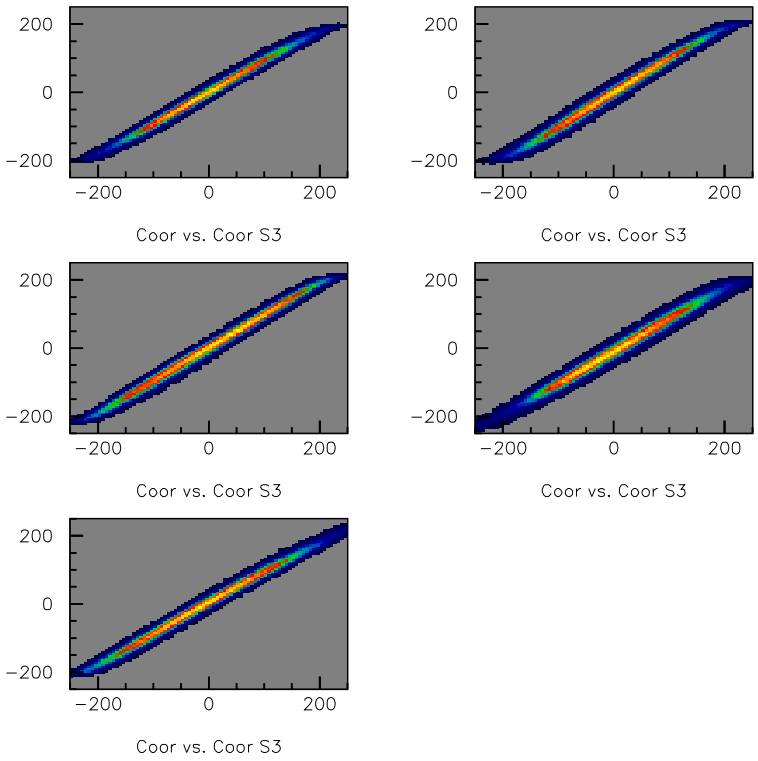

Figure 34: Coordinate as determined by the TDC time difference plotted vs. the coordinate as determined by the ADC ratio (units in cm). These data are from five counters of panel-2 S3.

7 Summary

The refurbishment of the CLAS TOF panel-1 and panel-2 counters into the new CLAS12 FTOF panel-1a and panel-2 counters took place in the period from May 2012 to May 2013. In this period the individual scintillation counters were repaired and tested extensively and mounted onto their associated support frames. Then extensive cosmic ray testing studies were carried out to determine the high voltage settings to gain match all of the PMTs and then the average time resolutions were measured for groups of three counters called triplets. The counters have shown performance very similar to what was achieved in their initial baseline studies in 1994 and 1995. The FTOF panel-1a and panel-2 counter arrays are now ready for installation onto the Forward Carriage in Hall B.

Acknowledgments

The successful refurbishment work of the FTOF panel-1a and panel-2 counter arrays has been supported by a number of individuals. These include Bob Miller (engineering), Joe Guerra (design), Al Johnson (technician), Sergey Boyarinov (DAQ), Gegham Asyran (physicist), the Hall B technical crew, and the JLab cabling group.

References

[1] RTV 103 silicone rubber adhesive sealant.

[2] D.S. Carman, *FTOF PMT Test Results*, logbook.

[3] CLAS12 FTOF Database for Panel-1a and Panel-2 Testing:
`http://userweb.jlab.org/~carman/ftof/FTOF-panel-1a-2.xlsx`

[4] J. Guerra, *FTOF - Panel-1a Modification Instructions*:
`http://userweb.jlab.org/~carman/ftof/docs/ftof-panel1a-mods.pdf`

[5] J. Guerra, *Panel-1a Bridge Attachment Hole Drill Procedure*:
`http://userweb.jlab.org/~carman/ftof/docs/drill-template.pdf`

[6] J. Guerra, *Panel-2 Assembly*:
`http://userweb.jlab.org/~carman/ftof/docs/panel2-assembly.pdf`

[7] J. Guerra, *FTOF Cable Runs*:
`http://userweb.jlab.org/~carman/ftof/cabling/cabling-study-v6.pdf`

[8] UV Curing Glue datasheet:
`http://userweb.jlab.org/~carman/ftof/docs/uv-glue.pdf`

[9] FTOF pre-installation QA data runs located on the silo at: /w/mss/clas/test

[10] J.E. Moyal, *Theory of Ionization Fluctuations*, Phil. Mag. **46**, 263 (1955). This approximation to the Landau form fits the peak region well but tends to slightly undershoot the tail of the distribution.

[11] E.S. Smith *et al.*, Nucl. Inst. and Meth. A **432**, 265 (1999).

[12] E.S. Smith and R. Nasseripour, CLAS-Note 2002-007, (2002).

[13] E.S. Smith, *Determination of Time-Walk Constants for the TOF Counters Using Thru Tracks*, GlueX-doc-1719, (2011).

[14] BC-408 Specification Sheet, Saint-Gobain Crystals:
`http://userweb.jlab.org/~carman/ftof/docs/scint-spec-sheet.pdf`